Pesticide Biochemistry and Physiology 184 (2022) 105066

Contents lists available at ScienceDirect

Pesticide Biochemistry and Physiology

journal homepage: www.elsevier.com/locate/pest

Co-encapsulation of *Pimpinella anisum* and *Coriandrum sativum* essential oils based synergistic formulation through binary mixture: Physico-chemical characterization, appraisal of antifungal mechanism of action, and application as natural food preservative

Somenath Das [a], Vipin Kumar Singh [b], Anand Kumar Chaudhari [b], Deepika [b], Abhishek Kumar Dwivedy [b], Nawal Kishore Dubey [b,*]

[a] Department of Botany, Burdwan Raj College, Purba Bardhaman, West Bengal 713104, India
[b] Laboratory of Herbal Pesticides, Centre of Advanced Study in Botany, Institute of Science, Banaras Hindu University, Varanasi 221005, India

ARTICLE INFO

Keywords:
Essential oil
Nanoemulsion
Antifungal
Aflatoxin B_1

ABSTRACT

The present study aimed to co-encapsulate binary synergistic formulation of *Pimpinella anisum* and *Coriandrum sativum* (PC) essential oils (0.75:0.25) into chitosan nanoemulsion (Nm-PC) with effective inhibition against fungal proliferation, aflatoxin B_1 (AFB_1) secretion, and lipid peroxidation in stored rice. Physico-chemical characterization of Nm-PC by SEM, FTIR, and XRD confirmed successful encompassment of PC inside the chitosan nanomatrix with efficient interaction by functional groups and reduction in crystallinity. Nm-PC showed superior antifungal, antiaflatoxigenic, and antioxidant activities over unencapsulated PC. Reduction in ergosterol biosynthesis and enhanced leakage of Ca^{2+}, K^{+}, Mg^{2+} ions and 260, 280 nm absorbing materials by Nm-PC fumigation confirmed irreversible damage of plasma membrane in toxigenic *Aspergillus flavus* cells. Significant diminution of methylglyoxal in *A. flavus* cells by Nm-PC fumigation illustrated biochemical mechanism for antiaflatoxigenic activity, suggesting future exploitation for development of aflatoxin resistant rice varieties through green transgenic technology. In silico findings indicated specific stereo-spatial interaction of anethole and linalool with Nor-1 protein, validating molecular mechanism for AFB_1 inhibition. In addition, in situ investigation revealed effective protection of stored rice against fungal occurrence, AFB_1 biosynthesis, and lipid peroxidation without affecting organoleptic attributes. Moreover, mammalian non-toxicity of chitosan entrapped PC synergistic nanoformulation could provide exciting potential for application as eco-smart safe nano-green food preservative.

1. Introduction

Fungi are opportunistic contaminant of food commodities, basically cereals, in the storage conditions leading to deterioration of nutritional qualities by production of different toxic secondary metabolites (mycotoxins), thereby, becoming a burning issue in 21st century (Shanakhat et al., 2018; Devi et al., 2021). *Aspergillus flavus* is one of the most common and competent fungal species, frequently contaminate rice (*Oryza sativa* L.) during postharvest storage by sporulation and production of aflatoxin B_1 (AFB_1), especially in tropical and subtropical regions of the world (Das et al., 2021a). Recent investigation of Food and agricultural organization (FAO) suggested approximate 15% loss of harvested rice due to improper storage resulting in fungal and AFB_1 contamination (Al-Zoreky and Saleh, 2019). More importantly, International agency for research on cancer (IARC) has categorized AFB_1 as class 1 human carcinogen on the basis of mutagenic, immunosuppressive, teratogenic and carcinogenic properties. Methylglyoxal, a reactive carbonyl component produced as a degradation product of glyceraldehyde 3-phosphate and dihydroxy acetone phosphate has shown major deleterious effects on foods during storage by inducing the AFB_1 biosynthesis and generation of advanced glycation end products (Upadhyay et al., 2018).

Although, the deployment of chemical preservative easily inhibit the contamination of fungi and their associated aflatoxins in foods during

* Corresponding author.
E-mail address: nkdubeybhu@gmail.com (N.K. Dubey).

https://doi.org/10.1016/j.pestbp.2022.105066
Received 23 November 2021; Received in revised form 6 February 2022; Accepted 23 February 2022
Available online 28 February 2022

storage conditions, however, overuse of these synthetic chemicals may result in increasing pathogen resistance, adverse health effects and environmental non-sustainability which made the food scientist to shift their idea towards the plant based products (Nikkhah and Hashemi, 2020). In this context, application of essential oils has been progressively emphasized for preparation of green fungicides based on their less residual toxicity, volatile nature, and mammalian non-toxicity. However, utilization of higher doses of essential oils during practical application in food commodities provides unfavorable organoleptic properties (due to absorption of essential oil components), therefore, optimization of dosage concentration are very important. Recently, use of essential oils in combination or formulation has been practiced in different food and agricultural industries due to their synergistic effects and significant antifungal activity at very low concentrations (Songsamoe et al., 2017). Binary mixture of essential oils has special benefit for their synergistic action and maximum participation of major components of different essential oils (Reyes-Jurado et al., 2019) with wide scale practical applicability in food industries for mitigation of fungal, aflatoxins and oxidative biodeterioration mediated postharvest problem of food commodities.

Inspite of proven antifungal efficacy of essential oils and combinations, their practical application is non-economical and limited due to easy degradation of volatile components by environmental factors like heat, oxygen, light and pressure, aqueous phase insolubility and volatile nature (Gavahian et al., 2020). Nanoencapsulation is a novel cutting edge advantageous technology for entrapment of essential oils/formulations inside any biopolymer facilitating controlled as well as targeted delivery with enhanced bioefficacy in food system. Among different synthetic and natural polymers, chitosan (a cationic polysaccharide extracted by deacetylation of chitin) is effectively used as nanoencapsulant or wall material in food and pharmaceutical industries due to biocompatibility, biodegradability, non-toxic nature, easy binding ability, better electrostatic interaction with negatively charge molecules, film, gel, and emulsion forming properties and more importantly, consideration under GRAS category (Das et al., 2021b). Plenty of researches have been performed on nanoencapsulation of essential oils; however, the electrostatic interaction based ionic gelation coupled with high speed homogenization and sonication produce nano-range emulsionic particles, better aqueous phase dispersibility, physical stability and controlled delivery, a prerequisite for stored food preservation against fungal infestation and aflatoxin contamination.

Myristica fragrans is a commonly cultivated aromatic spice plant in Asiatic and European countries as flavoring agent and condiments. Essential oil isolated from seeds, seed coats and fruits (MFEO) showed antimicrobial, hepatoprotective, anti-inflammatory, carminative, spasmolytic and antioxidant properties (Piaru et al., 2012). *Coriandrum sativum* is an herbaceous plant usually grown in Middle East and Mediteranean regions of the world. Essential oil of *C. sativum* (CSEO) is effective against fungi, bacteria, dyspepsia, diarrhea and digestive disorders (Burdock and Carabin, 2009). *Pimpinella anisum* is an annual aromatic and medicinal herb cultivated in Mediteranean area of Asia as flavoring agent and essential oil (PAEO) is used as diuretic, neuroprotective, antiulcer, and anticonvulsant effects (Hashem et al., 2018). *Anethum graveolens* is an herbaceous medicinal plant and essential oil isolated from different plant parts (AGEO) is widely used as antifungal, antidiabetic, antihyperlipidemic, and antisecretory properties (Kaur et al., 2019). To date, few reports are available regarding antifungal activity of MFEO, CSEO, PAEO and AGEO, however, essential oil formulation based on binary mixture combination with potential fungitoxic efficacy against food contaminating fungi, aflatoxin secretion, and enhancement in overall biological efficacy after chitosan based nanoencapsulation, especially focusing on biochemical and molecular mechanisms are completely lacking.

Hence, the aim of the present investigation was to prepare binary formulation of effective essential oils by checkerboard assay and co-encapsulation of the most effective binary synergistic formulation into chitosan nanomatrix with resultant enhancement in antifungal and antiaflatoxigenic activities. More importantly, the study was focused on relevant biochemical and molecular mechanism associated with antifungal and AFB_1 inhibitory efficacy. In addition, in situ fungitoxic, AFB_1 inhibition, lipid peroxidation, and organoleptic property assessment of essential oil nanoformulation was also performed in rice as a model food system. Furthermore, safety profile of prepared nanoformulation was determined in animal model (mice) for its recommendation as safe, green, and smart preservative in food and agricultural industries.

2. Materials and methods

2.1. Chemicals and solvents

Potato dextrose agar (PDA), SMKY (Sucrose, 200 g; $MgSO_4$. 7 H_2O, 0.5 g; KNO_3, 0.3 g; yeast extract, 7 g), Methanol, acetonitrile, isoamylalcohol, perchloric acid ($HClO_4$), DPPH, ABTS, toluene, acetone, KOH, $K_2S_2O_8$, NaCl, thiobarbeturic acid (TBA), tricholoroacetic acid (TCA), HCl, chitosan, Tween-20, Tween-80, dichloromethane (DCM), diaminobenzene (DAB), n-heptane, and chloroform were procured from Sisco Research laboratory (SRL), Mumbai, India.

2.2. Fungal strains

AFB_1 producing strain of *Aspergillus flavus* (AF LHP R14) along with different food biodeteriorating fungi such as *A. candidus*, *A. luchuensis*, *A. sydowii*, *A. repens*, *Fusarium oxysporum*, *F. poae*, *Alternaria alternata*, and Mycelia sterilia isolated from stored rice were used as test fungal strains (Das et al., 2020).

2.3. Extraction of essential oils and chemical characterization

Fresh plants of *A. graveolens*, *P. anisum*, and *C. sativum* were collected from Botanical garden, Banaras Hindu University, Varanasi, India and seed coats of *M. fragrans* were procured from local market of Varanasi, India. Fresh plants and seed coats were subjected to hydrodistillation (4 h) and extracted essential oils were passed through anhydrous sodium sulfate for removal of extra water.

GC–MS analysis of MFEO, AGEO, PAEO, CSEO, and PC synergistic formulation were performed by Thermo Scientific 1300 gas chromatograph equipped with silica capillary column (30 m × 0.25 mm; film thickness 0.1 μm) and TSQ quadruple mass spectrophotometer. 1 μL of MFEO, AGEO, PAEO, CSEO, and PC synergistic formulation (diluted in 1 mL of toluene) were injected into GC column. Helium was used as carrier gas with flow rate 1 mL min^{-1} (split ratio 50:1). Column oven temperature was set to 70–250 °C at a rate of 3 °C min^{-1} and programmed to temperature increase up to 290 °C. Source and transfer line temperature were maintained at 220 °C. Ionization energy was 70 eV with mass scanning between 40 and 450 amu. Characterization of bioactive constituents was done on the basis of elution order, retention time, and relative retention indices using homologous series of n-alkane (C9 – C28 hydrocarbons) as standard. Components were identified on the basis of National Institute of Standard and Technologies (NIST) libraries.

2.4. Preparation of synergistic formulations of PAEO and CSEO: Binary mixtures

In order to prepare binary formulation, at first, antifungal efficacy of MFEO, AGEO, PAEO, and CSEO were performed against toxigenic AF LHP R14 strain. Required concentrations of MFEO, AGEO, PAEO, and CSEO were mixed with 10 mL PDA medium in Petri plate followed by inoculation of 10 μL spore suspension (1×10^4 spores) of AF LHP R14 strain. Control set did not contain MFEO, AGEO, PAEO, and CSEO. Inhibition of fungal growth was calculated by measuring the colony diameter (cm) of the fungi appeared in control and treatment sets over 7 days of incubation period at 27 ± 2 °C at B.O·D. incubator (Das et al.,

2019). In the present investigation, PAEO, and CSEO were selected for preparation of binary mixture due to their highest antifungal activities. For this, combinations of PAEO, and CSEO were prepared by checkerboard method to obtain fractional inhibitory concentration index (FIC) against most aflatoxigenic AF LHP R14 strain. Different volumes of PAEO, and CSEO combinations were mixed with 10 mL of SMKY medium followed by inoculation of 10 μL of AF LHP R14 spore suspension (1×10^4 spore) in conical flasks. Control did not contain PAEO and CSEO combinations. The flasks were arranged as follows: EO_A on the X axis and EO_B on the Y axis. The conical flasks were kept in B.O·D incubator for 7 days at 27 ± 2 °C. Calculation of FIC indices were done by summation of FIC_A and FIC_B ($FIC_A + FIC_B$). FIC_A and FIC_B were minimum concentration of EO_A and EO_B that did not permit the growth of AF LHP R14 strain. Calculation of FICs were based on the following formula

$$FIC_A = \frac{\text{Minimum inhibitory concentration of A in presence of B}}{\text{Minimum inhibitory concentration of A alone.}}$$

$$FIC_B = \frac{\text{Minimum inhibitory concentration of B in presence of A}}{\text{Minimum inhibitory concentration of B aolne}}$$

Where A, B = Selected essential oils (PAEO and CSEO)

FIC index (FICI) = $FIC_A + FIC_B$

Interpretation of different combinations of PAEO and CSEO were demonstrated as, synergistic effects (FICI <0.5); additive effects ($0.5 \leq FIC \leq 1$); no interactive effects ($1 < FIC \leq 4$); antagonistic effects (FIC > 4) (Lesjak et al., 2016).

2.5. Synthesis of binary mixture mediated synergistic formulation (PAEO+CSEO) loaded chitosan nanoemulsion (Nm-PC)

Ionic gelation protocol of Hasheminejad et al. (2019) with slight modification was used for preparation of synergistic formulation loaded chitosan nanoemulsion (Nm-PC). Chitosan solution (1.5%) was prepared in 1% glacial acetic acid by stirring overnight at 25–27 °C. Tween-80 (0.27 g) was added in the chitosan solution as surfactant for 45 min to form homogeneous mixture. Required volumes of PAEO and CSEO synergistic mixture (PC) (0.12, 0.24, 0.36, 0.48, and 0.60 g) was mixed with 4 mL DCM for preparation of 1:0, 1:0.2, 1:0.4, 1:0.6, 1:0.8 and 1:1 ratios of PC to chitosan. The oil phase of PC was gradually added to the chitosan solution at the time of homogenization (12,000 ×g for 13 min) using T18 Digital Ultra- Turrax, IKA homogenizer. 0.4% TPP was added drop-wise to the prepared chitosan emulsion and left for 40 min on magnetic stirrer (IKON IK-163, India) with continuous agitation. The emulsion was centrifuged at 10,000 ×*g* for 10 min (4 °C) and washed with double distilled water 2–3 times. Finally, sonication of the synthesized nanoemulsion was performed through ultrasonicator (Sonics Vibra Cell) for 4 min with 1 s pulse on and 1 s pulse off. The suspension was immediately lyophilized at −72 °C for 3 days to develop powder nanoparticle. The biological experiments were performed through prepared nanoemulsion, whereas, nanoparticles were used for physico-chemical characterizations.

2.6. Characterization of Nm-PC

2.6.1. Scanning electron microscopy (SEM)

Morphological features of chitosan nanoparticles and powdered Nm-PC particles were performed through SEM (Sigma, Zeiss SEM) after dissolving them into 1 mL of double distilled water and sonicated for 4 min. 5 μL of sonicated suspension was placed over clean cover slip, coated into gold sputter and image was observed at 20,000 to 50,000 × magnification.

2.6.2. Functional group analysis by Fourier transform infrared spectroscopy (FTIR)

Interaction between functional groups of chitosan, chitosan nanoparticle, PC, and Nm-PC nanoparticle were observed in Perkin Elmer FTIR in between wave number 500–5000 cm^{-1} with 32 scan and 4 cm^{-1} resolution.

2.6.3. Crystallinity study by X-ray diffractometry

Degree of crystallinity in chitosan, chitosan nanoparticle, and Nm-PC were measured through XRD (Bruker D8 Advance) between 2θ value 5–50° and step angle 0.04° min^{-1}.

2.7. Determination of encapsulation efficiency (EE), loading capacity (LC) and encapsulation yield (EY)

Spectrophotometric method was used for determination of encapsulation efficiency and loading capacity of Nm-PC. Absorption spectrum of PC was constructed in ethyl acetate at 267 nm. Amount of PC loaded in chitosan nanomatrix was measured after extracting PC into ethyl acetate. Briefly, 300 μL of Nm-PC was dissolved into 3 mL of ethyl acetate (added in a sequence of 1 + 1+ 1 mL), mixed properly and centrifuged at 10,000 ×*g* for 10 min. Absorbance of the collected supernatant was measured at wavelength of 267 nm and compared with the calibration curve ($R^2 = 0.975$). Chitosan nanoemulsion without addition of PAEO and CSEO mixture served as blank. EE and LC were measured on the basis of following formula

$$\%EE = \frac{\text{Amount of loaded PAEO and CSEO mixture}}{\text{Initial amount of PAEO and CSEO mixture}} \times 100$$

$$\%LC = \frac{\text{Total amount of loaded PAEO and CSEO mixture}}{\text{Weight of nanoemulsion}} \times 100$$

EY of lyophilized nanoparticle was determined only for maximum percent loading capacity of chitosan to PC (1:0.8 *w/v*).

$$\%EY = \frac{\text{Weight of freeze dried nanoparticle}}{\text{Sum total weight of freeze dried initial contents}} \times 100$$

2.8. In vitro release profile of Nm-PC

Briefly, 300 μL of Nm-PC was dissolved into 5 mL of solution mixture containing phosphate buffer saline (PBS, pH 7.4) and ethanol (3:2 *v*/v) followed by gentle agitation for 10–15 min. At specific intervals of time (0–192 h), centrifugation of the sample was performed at 8000 ×*g* for 10 min. 200 μL of collected supernatant was mixed with PBS and ethanol mixture followed by measurement of absorption at 267 nm. All the time, fresh PBS was added to maintain the total volume (Hosseini et al., 2013). Content of PC released was calculated using standard calibration curve ($R^2 = 0.975$). Cumulative release of PC from chitosan nanoemulsion was measured through the following formula

$$\text{Cumulative release of PC} = \frac{\text{PC released at each sampling time}}{\text{Initial weight of PC loaded in the sample}} \times 100$$

2.9. Antifungal and AFB_1 inhibitory effectiveness of PC and Nm-PC

Briefly, desired amounts of PC (0.05, 0.1, 0.15 and 0.2 μL/mL) and Nm-PC (0.01, 0.02, 0.03, 0.04, 0.05, and 0.06 μL/mL) were amended with 25 mL SMKY medium followed by addition of 25 μL AF LHP R14 spore suspension (2.5×10^4 spores). Controls were prepared without the addition of PC and Nm-PC into SMKY medium. The control and treatments sets were left in B.O·D incubator at 27 ± 2 °C for 10 days. Concentrations representing complete inhibition of AF LHP R14 cells growth (in terms of % inhibition) by PC and Nm-PC were reported as minimum

inhibitory concentrations (MICs). Fungitoxic spectrum of PC and Nm-PC against *A. candidus*, *A. luchuensis*, *A. sydowii*, *A. repens*, *Fusarium oxysporum*, *F. poae*, *Alternata alternata*, and Mycelia sterilia were performed at MIC doses after inoculation with 5 mm fungal discs in PDA medium. Percent inhibition of fungal growth was calculated by following formula.

$$\text{Inhibition } (\%) = \frac{\text{Fungal colony diamter in control} - \text{Fungal colony diameter in treatment}}{\text{Fungal colony diameter in control}} \times 100$$

To find out the AFB_1 inhibitory potential, media of control and treatment sets were filtered through muslin cloth and extracted into 20 mL chloroform in separating funnel. The chloroform extract was evaporated to dryness over water-bath at 85 °C for 4 h. The residue left was mixed with 1 mL of methanol and 50 μL of methanolic extract was spotted on thin layer chromatography (TLC) plate and developed in MTI solution (methanol, toluene and isoamylalcohol; 2:90:32 *v*/v/v). Blue spots (as observed through UV-transilluminator) were scrapped from TLC plate and added to 5 mL methanol and centrifuged at 5000 ×*g* for 10 min. The optical density of the collected supernatant was measured at 365 nm. Calculation of AFB_1 content was done by following formula

$$AFB_1 \text{ content } (\mu g/mL) = \frac{\text{Molecular weight of } AFB_1 \times \text{Optical density at 365 nm}}{\text{Path length} \times \text{Molar extinction coefficient of } AFB_1} \times 1000$$

Concentration of PC and Nm-PC showing 100% inhibition of AFB_1 was observed as minimum AFB_1 inhibitory concentration (MAIC).

2.10. Mechanism involving antifungal and AFB_1 inhibition

2.10.1. Biochemical mechanisms

2.10.1.1. Ergosterol quantification by fumigation with PC and Nm-PC. Protocol of Chaudhari et al. (2020) was adopted for extraction of ergosterol from AF LHP R14 cells after fumigation with PC and Nm-PC. Required amounts of PC (0.05, 0.1, 0.15 and 0.2 μL/mL) and Nm-PC (0.01, 0.02, 0.03, 0.04, 0.05 and 0.06 μL/mL) were mixed with 25 mL of SMKY medium followed by inoculation with 25 μL AF LHP R14 spore suspension (2.5×10^4 spores) and kept in B.O·D incubator at 27 ± 2 °C for 4 days. Controls sets were devoid of PC and Nm-PC. After completion of incubation, the autoclaved AF LHP R14 biomass was weighed and mixed with 5 mL 25% ethanolic KOH solution. Thereafter, fungal biomass was heated over water bath for 2 h at 85 °C. Extraction of ergosterol was done by addition of n-heptane and water mixture (5:2 *v*/v) followed by vortex mixing and proper separation of two distinct layers. The upper n-heptane layer was collected and scanned spectrophotometrically between 230 and 300 nm. Ergosterol content was determined by the following formula.

$$\%\text{Ergosterol} + \%24\ (28)\ \text{dehydroergosterol} = \left(\frac{\text{Absorbance at 281.5 nm}}{290}\right) \Big/ \text{Pellet weight}$$

$$\%24\ (28)\ \text{dehydroergosterol} = \left(\frac{\text{Absorbance at 230 nm}}{518}\right) \Big/ \text{Pellet weight}$$

$$\%\text{Ergosterol} = [\%\text{Ergosterol} + \%24\ (28)\ \text{dehydroergosterol}] - \%24\ (28)\ \text{dehydroergosterol}$$

290 and 518 are E values (percentage/cm) for ergosterol and 24 (28) dehydroergosterol.

2.10.1.2. Effect on ions and 260, 280 nm absorbing materials leakage. Seven days grown biomass of AF LHP R14 cells were washed with sterile distilled water and fumigated with ½ MIC, MIC, and 2 MIC doses of PC (0.1, 0.2, and 0.4 μL/mL) and Nm-PC (0.03, 0.06, and 0.12 μL/mL) in 0.85% saline solution. Control sets were devoid of PC and Nm-PC fumigation. Both control and treatment sets were incubated for 16 h at B.O·D incubator at 27 ± 2 °C. Thereafter, the biomass was filtered and filtrate was used for determination of Ca^{2+}, K^{+} and Mg^{2+} ions and 260, 280 nm absorbing material through atomic absorption spectroscopy and UV–Visible spectroscopy, respectively.

2.10.1.3. Effect on cellular methylglyoxal (AFB_1 inducing substrate). Methylglyoxal content in AF LHP R14 cells was determined following the methodology of Yadav et al. (2005). 0.3 g of harvested fungal biomass (7 days old AF LHP R14 cells) was fumigated with ½ MIC, MIC and 2 MIC doses of PC (0.1, 0.2, and 0.4 μL/mL) and Nm-PC (0.03, 0.06, and 0.12 μL/mL) into 10 mL SMKY medium. Control sets were devoid of PC and Nm-PC treatment. Control and fumigated sets were incubated for 16 h in B.O.D incubator at 27 ± 2 °C. Thereafter, AF LHP R14 biomass was crushed into 3 mL of 0.5 M perchloric acid followed by centrifugation at 11000 ×*g* for 10 min (4 °C). Supernatant was collected and neutralized by K_2CO_3 solution. The neutralized supernatant was further centrifuged at 11,000 ×*g* for 10 min and estimation of methylglyoxal was done by using the collected supernatant. Methylglyoxal content was determined by sequential addition of 1,2 diamino benzene, 5 M perchloric acid and neutralized supernatant and optical density was measured at 336 nm. Amount of methylglyoxal was calculated by comparing with standard curve and expressed as μM/gFW.

2.10.2. Molecular mechanism for target site determination

2.10.2.1. In silico molecular modeling of anethole and linalool against Nor-1 protein. Nor-1 protein sequence in FASTA format was retrieved from UniProt data base for proteins and converted into three dimensional structure (3D) by Phyre 2 online server. 3D structures of major components of PC viz. anethole and linalool were downloaded from PubChem data base. Patch dock online server was utilized for binding of anethole and linalool with Nor-1 protein and 20 best models were prepared through Fire dock software on the basis of different interactive energy indices such as global energy, attractive vander Waal, repulsive vander Waal force and atomic contact energy. The components and Nor-1 protein interactions were presented through PyMol and Discovery

Studio software.

2.11. Assessment of antioxidant activity

Antioxidant activity of PAEO, CSEO, PC, chitosan nanoemulsion and Nm-PC were determined through DPPH• and ABTS•$^{+}$ assay. For DPPH radical quenching assay, required volumes of PAEO, CSEO, PC, chitosan nanoemulsion and Nm-PC were mixed with 0.004% DPPH solution (5 mL) and absorbance was recorded at 517 nm after 30 min of incubation in dark. Percent scavenging effect was measured by the following equation

$$\text{Scavenging effect } (\%) = 1-\frac{\text{Absorption of sample}}{\text{Absorption of control}} \times 100$$

ABTS•$^{+}$ radical cations were developed by sequential addition of ABTS (7 mmol L^{-1}) and $K_2S_2O_8$ (2.45 mmol L^{-1}) followed by incubation in dark for 12–16 h. The prepared mixture was diluted with absolute ethanol until absorbance of mixture maintained to 0.7 ± 0.05 at 734 nm. Different concentrations of PAEO, CSEO, PC, chitosan nanoemulsion, and Nm-PC were dissolved into 2 mL of ABTS•$^{+}$ reaction mixture and incubated in dark for 6 min. After reaction, absorbance was recorded at 734 nm and scavenging effect was measured by the same equation of DPPH assay.

2.12. In situ efficacy of PC and Nm-PC against fungal infestation and AFB_1 contamination in rice (the model food system): high performance liquid chromatography (HPLC) analysis

Briefly, 250 g of rice seeds were fumigated with PC and Nm-PC in plastic container and stored for 1 year at 25–30 °C and RH ~ 30–80%. Two different control and treatment sets viz. uninoculated control, inoculated control, uninoculated treatment and inoculated treatment were prepared on the basis of inoculation of 500 μL spore suspension. Treatment of PC and Nm-PC in rice seeds were performed at MIC (0.2, 0.06 μL/mL) and 2 MIC (0.4, 0.12 μL/mL) doses. After completion of storage periods, mycoflora analysis of rice seeds was performed by serial dilution. For serial dilution, 1 g of grinded rice seeds was mixed with 9 mL of double distilled water and mixed properly. 1 mL aliquot of 10^{-4} dilution was spread over PDA medium in Petri plates by sterile L-shaped spreader. Thereafter, Petri plates were incubated for 7 days at 27 ± 2 °C. Colonies of different fungi were noted and percent protection against fungal infestation was calculated by following formula

$$\%\text{Fungal protection} = \frac{\text{Number of fungal colony in control} - \text{Number of fungal colony in treatment}}{\text{Number of fungal colony in control}} \times 100$$

Amount of AFB_1 in rice was determined by mixing 1 g of crushed rice seeds in reaction mixture containing distilled water and methanol (10:8 *v*/v) in conical flask. Thereafter, the crushed rice samples were agitated in mechanical shaker at 400 ×g for 30 min. Collected samples were centrifuged at 3000 ×*g* for 10 min (4 °C). Four milliliter of collected supernatant was mixed with 300 μL of chloroform in centrifuge tube followed by addition of 6 mL 3% KBr mixed water. Further, centrifugation of the mixture was performed at 3000 ×*g* for 10 min and lower settled phase was collected into microcentrifuge tube. Microcentrifuge tube containing solution mixture was evaporated to dryness over water bath at 85 °C for 2 h. After completion of drying, elute left was mixed with 1 mL of HPLC grade methanol and filtered to remove the suspended impurities. Thereafter, 50 μL of sample was injected into C-18 reverse phase column (250 mm × 4.6 mm × 5 μm) using mobile phase of distilled water, acetonitrile, and methanol (64:19:17 v/v/v) with flow rate 1.2 μL/min. Limit of detection (LOD) in HPLC system was recorded in between 12.5 and 500 ng/50 mL. AFB_1 content was detected at excitation wavelength of 365 nm (Sheijooni-Fumani et al., 2011).

2.13. Effect on lipid peroxidation of rice seeds

Extent of lipid peroxidation in rice seeds were measured by malondialdehyde (MDA) assay following the protocol of Buege and Aust (1978). For this, 1 g of grinded rice seeds were dissolved into TBA-TCA-HCl reagent mixture (prepared by subsequent mixing of 15% TCA, 0.375% TBA and 0.25 N HCl) followed by subjection of mild heat over water-bath for 20 min. Thereafter, cooling of samples were performed in running tap water and centrifuged at 5000 ×*g* for 10 min to remove the precipitate. Absorbance of collected supernatant was recorded at 532 nm followed by subtraction of non-specific absorbance at 600 nm against a blank that contained all the reagents except grinded rice by UV–Visible spectrophotometer. MDA content was determined in rice samples in terms of μM/gFW by using the extinction coefficient 1.56 × 10^5 M^{-1} cm^{-1}.

2.14. Effect on organoleptic properties of rice seeds

The experiment to analyze the effect of PC and Nm-PC on organoleptic properties of rice was conducted on the basis of previous researcher's studies (Clemente et al., 2019; Kumar et al., 2020; Deepika et al., 2021; Chaudhari et al., 2022). However, there may be minor differences in the methodology reported by investigators. Assessment of organoleptic properties (odor, texture, color and flavor) in rice by fumigation with PC and Nm-PC were performed by 10 different experienced panelists (5 male and 5 female) from Banaras Hindu University, Varanasi, India aged between 25 and 50 years. The panelists were informed about the methodology and asked to sign a consent form pertaining to the reagents used for preparation of nanoemulsion and allergic reactions. Three minute was provided to each panelist for answering of different organoleptic properties. The gap between samples was 5 min. Scoring of organoleptic properties was presented on the basis of 5 point hedonic scale viz. 1 = extremely dislike, 2 = moderately dislike, 3 = neither like nor dislike, 4 = moderately like and, 5 = extremely like. Rice samples receiving score above 4 for all the organoleptic properties were recorded as acceptable limit.

2.15. Assessment of LD_{50} in mice (animal model)

Safety level evaluation of PC and Nm-PC was done in mice model following the rules and regulations of Animal care and Ethical Committee, Banaras Hindu University, Varanasi, India. Three months old male mice (average weight 29.63 g) were collected from Institute of Medical Science, Banaras Hindu University and kept in laboratory for one week to acclimatize the condition. Different doses of PC (100, 200, 300, 400, 500 and 600 μL/kg body weight) and Nm-PC (50, 100, 150, 200, 250, and 300 μL/kg body weight) were subjected to oral administration in each mice group (10 mice in one group) by micropipette catheter. Control mice groups did not administer with PC and Nm-PC, however only possess Tween-20 and double distilled water. Mortality rate was determined within 24–48 h by Probit analysis and represented by the LD_{50} value.

Table 1
GC–MS analysis of MFEO, AGEO, PAEO, CSEO and (PAEO+CSEO) combination.

S.No.	Retention time	Components	% compositions					Retention Index
			MFEO	AGEO	CSEO	PAEO	PAEO + CSEO (PC) 0.75:0.25 combination	
1.	4.17	α-Thujene	–	0.14	–	–	–	930
2.	4.38	α-pinene	0.84	–	0.85	1.02	3.41	939
3.	4.46	Camphene	1.61	–	–	0.87	–	954
4.	6.20	D-Limonene	–	6.89	2.69	6.20	4.98	1029
5.	6.38	1,8 cineol	–	2.38	–	1.51	–	1031
6.	6.50	O-cymene	–	–	0.58	–	–	1026
7.	8.85	Linalool	–	–	72.51	–	41.89	1096
8.	9.97	Camphor	–	–	–	0.41	–	1146
9.	10.78	Citronellal	–	–	0.12	–	–	1153
10.	11.63	α-Terpinenyl acetate	2.15	0.98	1.03	–	–	1171
11.	11.65	*P*-Cymene	–	2.94	–	–	–	1187
12.	12.08	Estragole	–	–	–	19.51	7.98	1196
13.	12.42	α-Phellandrene	3.20	–	–	–	–	1202
14.	12.51	α-terpineol	3.98	–	0.88	–	0.36	1228
16.	13.47	Linalyl acetate	0.99	–	–	–	–	1240
17.	13.70	Carvone	–	21.20	–	1.02	0.48	1257
18.	14.42	Fenchone	–	1.20	–	16.89	3.45	1286
19.	14.54	*P*-Cymenene	–	0.11	–	–	–	1291
20.	15.54	Anethole	–	10.54	4.13	41.41	20.87	1352
21.	16.56	Undecanal	–	–	0.63	–	0.28	1306
22.	18.94	3-Thujanol	10.63	–	–	–	–	1368
23.	19.81	Geranyl acetate	–	–	7.10	–	8.89	1381
24.	19.603	*Cis*-Dihydrocarvone	–	0.52	–	–	–	1392
25.	19.83	*Trans*-Dihydrocarvone	–	1.25	–	–	–	1400
26.	20.51	Dodecanal	–	–	1.32	–	–	1408
27.	24.00	Safrole	4.69	–	–	–	–	1487
28	26.88	α-Patchoulene	1.40	0.36	–	–	–	1456
29.	29.24	Methyl eugenol	3.56	–	–	–	–	1489
30.	29.40	Asarone	–	–	1.03	1.26	1.74	1574
31.	34.44	Myristicin	24.78	1.56	–	–	–	1518
32.	35.51	Elemicin	33.69	0.09	–	–	–	1557
33.	36.68	Carotol	–	1.02	–	–	–	1594
34.	38.05	Dill apiole		40.87			–	1620
Total			**91.52**	**92.05**	**92.87**	**90.10**	**94.33**	

Table 2
Antifungal efficacy testing of MFEO, AGEO, PAEO and CSEO against *A. flavus* (AF LHP R14) strain.

Concentration of MFEO (μL/mL)	% Inhibition of AF LHP R14 growth	Concentration of AGEO (μL/mL)	% Inhibition of AF LHP R14 growth	Concentration of PAEO (μL/mL)	% Inhibition of AF LHP R14 growth	Concentration of CSEO (μL/mL)	% Inhibition of AF LHP R14 growth
CNT	0.00 ± 0.00^{a}	CNT	0.00 ± 0.00^{a}	CNT	0.00 ± 0.00^{a}	CNT	0.00 ± 0.00^{a}
0.25	2.09 ± 0.47^{b}	0.2	14.39 ± 1.19^{b}	0.1	10.31 ± 1.74^{b}	0.1	8.29 ± 0.57^{b}
0.50	6.10 ± 0.11^{c}	0.4	20.67 ± 1.12^{c}	0.2	23.08 ± 1.59^{c}	0.2	17.08 ± 1.06^{c}
0.75	13.06 ± 0.97^{d}	0.6	39.52 ± 2.01^{d}	0.3	38.45 ± 3.18^{d}	0.3	25.97 ± 3.01^{d}
1.0	22.52 ± 1.03^{e}	0.8	55.10 ± 1.29^{e}	0.4	52.14 ± 2.43^{e}	0.4	39.32 ± 2.09^{e}
1.25	38.10 ± 2.02^{f}	1.0	71.26 ± 3.08^{f}	0.5	67.20 ± 1.17^{f}	0.5	47.12 ± 3.39^{f}
1.50	50.10 ± 2.36^{g}	1.2	89.21 ± 1.87^{g}	0.6	79.97 ± 4.19^{g}	0.6	55.57 ± 4.18^{g}
1.75	61.03 ± 4.01^{h}	1.4	96.35 ± 2.82^{h}	0.7	87.21 ± 2.09^{h}	0.7	67.31 ± 3.97^{h}
2.0	75.21 ± 4.44^{i}	1.6	100 ± 0.00^{i}	0.8	93.01 ± 3.33^{i}	0.8	79.19 ± 2.19^{i}
2.25	82.11 ± 3.10^{j}			0.9	100 ± 0.00^{j}	0.9	85.96 ± 3.74^{j}
2.50	88.40 ± 1.02^{k}					1.0	91.06 ± 5.79^{k}
2.75	93.12 ± 1.65^{l}					1.1	98.30 ± 3.17^{l}
3.0	96.10 ± 3.17^{m}					1.2	100 ± 0.00^{m}
3.5	100 ± 0.00^{n}						

Note: Values are mean (n = 3) ± SE, the means followed by same letter in the same column are not significantly different according to ANOVA and Tukey's multiple comparison tests.

2.16. Statistical analyses

Experiments were done in triplicate and data evaluation was performed through mean ± standard error format along with analysis of variance (ANOVA) coupled to Tukey's B coefficient and significant differences at $P < 0.05$. Graphs were prepared in Microsoft Windows Excel 2019, Sigma Plot, and SPSS (Version18.0, SPSS Inc. Chicago, USA) soft ware.

3. Results and discussion

3.1. Extraction of MFEO, AGEO, PAEO, CSEO and their chemical characterizations

Fresh plants of *A. graveolens*, *P. anisum*, *C. sativum* and seed coats of *M. fragrans* were used for extraction of AGEO, PAEO, CSEO, and MFEO, respectively. GC–MS of MFEO revealed elemicine, and myristicine as major components. A total of 16 components were found in GC–MS of AGEO; among them, dill apiol, and carvone were reported as major components. Chemical characterization of CSEO presented 12

Table 3
Different combination of PAEO and CSEO binary mixture (PC) and their effect against growth of toxigenic AF LHP R14 cells.

Essential oil combination (ratio)		% inhibition of AF LHP R14 growth	FIC index (FICI)	Interactive effects
PAEO	CSEO			
0	0	0.00 ± 0.00^{a}	–	–
0	0.25	8.48 ± 0.43^{b}	–	–
0.25	0	11.48 ± 0.46^{b}	–	–
0.25	0.25	29.70 ± 0.62^{e}	0.69	Additive
0.25	0.50	81.74 ± 1.01^{lm}	0.31	Synergistic
0.25	0.75	72.25 ± 0.84^{hi}	0.84	Additive
0.25	1.0	78.49 ± 0.60^{jkl}	0.73	Additive
0	0.50	10.05 ± 0.43^{b}	–	–
0.50	0	39.51 ± 0.48^{f}	–	–
0.50	0.25	70.16 ± 2.81^{h}	0.39	Synergistic
0.50	0.50	84.17 ± 1.78^{mn}	0.28	Synergistic
0.50	0.75	75.30 ± 3.83^{ij}	0.61	Additive
0.5	1.0	80.46 ± 1.44^{klm}	0.42	Synergistic
0	0.75	17.52 ± 1.52^{c}	–	–
0.75	0	23.97 ± 2.03^{d}	–	–
0.75	**0.25**	**$100 \pm 0.00^{P*}$**	**0.29**	**Synergistic**
0.75	0.5	84.41 ± 1.23^{mn}	0.85	Additive
0.75	0.75	90.18 ± 3.78^{o}	0.36	Synergistic
0.75	1.0	70.28 ± 1.02^{h}	0.71	Additive
0	1.0	21.40 ± 2.73^{d}	–	–
1.0	0	87.82 ± 1.79^{no}	–	–
1.0	0.25	76.83 ± 1.10^{ijk}	0.83	Additive
1.0	0.5	84.02 ± 1.29^{n}	0.40	Synergistic
1.0	0.75	64.06 ± 1.52^{m}	0.77	Additive
1.0	1.0	90.82 ± 2.03^{o}	0.26	Synergistic

Note: - = Not determined due to involvement of single essential oil, * = Maximum inhibition of AFLHPR14 growth with synergistic activity. Values are mean (n = 3) ± SE, the means followed by same letter in the same column are not significantly different according to ANOVA and Tukey's multiple comparison tests.

components, among them, linalool and geranyl acetate were found as major ingredient. GC–MS of PAEO revealed 10 components, among them, anethole and estragol were reported as major components (Table 1). As maximum synergism was achieved for 0.75:0.25 combination of PAEO and CSEO (PC) (data presented in section 3.2.), hence, GC–MS analysis of PC binary synergistic mixture was also performed. PC revealed the presence of linalool, anethole, estragol and geranyl acetate as major component (Table 1) confirming successful preparation of binary synergistic formulation. Variation in essential oil components are depended on alteration in geographical regions, climatic, edaphic factors, chemotypic alteration, plant parts used for extraction of essential oil, changing functionality in limonene synthase gene during terpenoid sysnthesis and more importantly, synergistic activity of major and minor components (Houicher et al., 2018; Bahmankar et al., 2019). In addition, environmental factors (humidity, light, and temperature), types of soil, and their interaction with nutrient availability ecophysiology as well as growth stage of plants significantly influence the compositional variation in essential oil (Walia et al., 2020). Hence, validation of chemical composition of binary synergistic formulation is an important parameter to be considered before investigating broad scale antifungal and antiaflatoxigenic efficacy.

3.2. Preparation of synergistic formulation of PAEO and CSEO: binary mixture

In the present investigation, antifungal efficacy of MFEO, AGEO, PAEO and CSEO against aflatoxigenic AF LHP R14 strain was assessed (Table 2). Among different tested essential oils, PAEO and CSEO showed 100% inhibition of fungal growth at very lower doses (0.9 and 1.2 μL/mL, respectively). Hence, in the present piece of work, binary mixture assay of PAEO and CSEO was adopted for preparation of synergistic antifungal formulation. Synergism of essential oils achieved better biological efficacy in food system as compared to their joint additive actions, therefore, we have intended to focus on selection of maximum synergistic activity of binary mixture of test essential oils. Different formulations of PAEO and CSEO were prepared by mixing varying ratios (prepared by checker board) viz. 0.00:0.00, 0.00:0.25, 0.25:0.00, 0.25:0.25, 0.25:0.50, 0.25:0.75, 0.25:1.0, 0.00:0.50, 0.50:0.00, 0.50:0.25, 0.50:0.50, 0.50:0.75, 0.5:1.0, 0.00:0.75, 0.75:0.00, 0.75:0.25, 0.75:0.50, 0.75:0.75, 0.75:1.0, 0.00:1.00, 1.00:0.00, 1.00:0.25, 1.00:0.50, 1.00:0.75 and 1.00:1.00 (Table 3). Growth status of AF LHP R14 cells in presence of different formulations was recorded in terms of percent inhibition. FIC Index of different formulations was calculated on the basis of minimum inhibitory concentrations of PAEO and CSEO. In case of 0.75:0.25 combination of PAEO and CSEO (PC), maximum synergism was achieved (FICI = 0.29) with highest inhibition of aflatoxigenic AF LHP R14 cells growth (100%) (Table 3). Synergistic activity of PC has been attributed due to interaction of major and minor components of CSEO and PAEO as confirmed through GC–MS analysis. Similar synergistic effects by mixing varied combination of Thyme, Rosemary, Marjoram and Cinnamon essential oils with effective inhibition of *Botrytis cineria* and *Penicillium expansum* infestation in pear fruits has been demonstrated by Nikkhah et al. (2017). However, our finding represented better synergistic efficacy of PC to mitigate broad range food contaminating fungi along with inhibition of toxigenic *A. flavus* cell growth and AFB_1 section.

3.3. Synthesis of PC synergistic formulation loaded chitosan nanoemulsion (Nm-PC)

PC synergistic formulation loaded chitosan nanoemulsion (Nm-PC) was synthesized via two step process involving the formation of PC droplets followed by solidification after ionic cross-linking of protonated amino group (NH_3^+) of chitosan with phosphoric ions (PO_4^{3-}) of S-TPP during subsequent homogenization and sonication. In our present investigation, selection of chitosan as encapsulating agent for successful entrapment of PC completely depends on ample sources with easy extraction, non-toxic nature, GRAS consideration and chemical modification possibility by electrostatic and hydrogen bonding of functional groups of S-TPP leading to production of novel nanometric variants such as emulsion, gel, nanofibre, nanoparticle, and nanocomposites (Hadidi et al., 2020). Moreover, Tween-80 was utilized as stabilizing agent, also facilitated in nanostructural compaction by reducing the surface energy of emulsion system culminating into development of sub-cellular size emulsionic particles. Different ratios of chitosan to PC (*w/v*) were used for selection of better entrapment ability of PC as a core material inside the chitosan biopolymer with maximum stability.

3.4. Characterization of Nm-PC

3.4.1. SEM analysis

Fig. 1 A, B presents the SEM image of unloaded chitosan nanoparticle and Nm-PC nanoparticle with mere rounded shapes, smooth surface and tendency to aggregate in some places. The roundish shape of particles may be ascribed due to immediate interaction of positive NH_3^+ group of chitosan with S-TPP facilitating sudden neutralization followed by particle formation (Barrera-Martínez et al., 2021). Size of emulsionic chitosan nanoparticles were in the range of 49.67–71.21 nm (Fig. 1 A), while, it can be clearly seen in the figure that after encompassment of PC into chitosan nanobiopolymer (Nm-PC), the particle size were reduced to 16.79–30.44 nm (Fig. 1 B). Decrement in particle size after entrapment of essential oil might be attributed due to application of Tween-80 as surfactant leading to greater compaction during ionotropic gelation. Our result is in corroboration with the finding of da Silva Gündel et al. (2018), while encapsulating the *Cymbopogon flexuosus* essential oil. Reduction in Nm-PC particle size is desirable in the present investigation because it would be associated with greater surface to volume ratio and

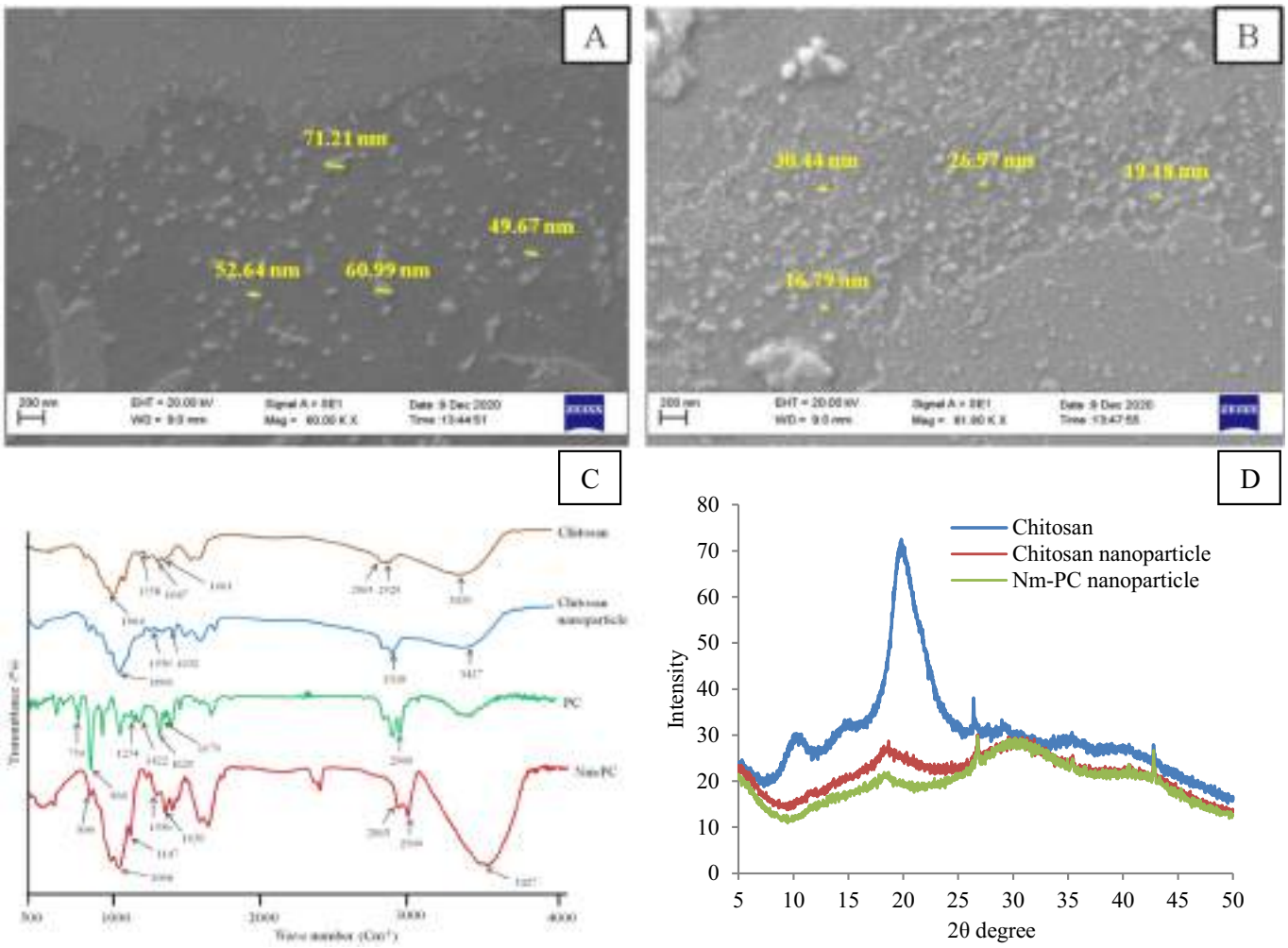

Fig. 1. SEM analysis of chitosan nanoparticle (A), Nm-PC nanoparticle (B), FTIR analysis of chitosan, chitosan nanoparticle, PC and Nm-PC nanoparticle (C), XRD analysis of chitosan, chitosan nanoparticle, and Nm-PC nanoparticle (D).

helpful for protection of stored rice against fungal infestation and immediate neutralization of biodeteriorating free radicals with subsequent inhibition of AFB_1 biosynthesis.

3.4.2. *Functional group analysis by FTIR*

FTIR spectra of chitosan, chitosan nanoparticle, PC and Nm-PC nanoparticle represent the availability of functional groups and their possible interaction during nanoemulsion synthesis. The result illustrated the characteristics peaks of chitosan powder at 664 (pyranoside ring), 1386 (C–O–C), 1380 (symmetrical deformation of CH), 1558 (amide-II), 1598 (–NH_2 bending vibration), 1638 (amide-I), 1647 (–$CONH_2$), 2865 (symmetrical stretching of CH), and 3420 cm^{-1} (combined NH_2/OH peak) (Fig. 1 C). As compared to chitosan powder, chitosan nanoparticle exhibited shifting of amide I and II peak to 1632 and 1530 cm^{-1}, respectively, clearly suggesting the involvement of –NH_2 groups in ionic interaction with S-TPP. Moreover, the peak of P═O group at 1066 also signified the S-TPP cross-linking with –NH_2 group of chitosan (Matshetshe et al., 2018). PC showed specific absorption band at 750, 866, 1254 (–CH and –CH_2 bending), 1422, 1620 (C═C group vibration), 1670 (C═O stretching), and 2960 (–CH stretching) cm^{-1}. It can be evident from figure that incorporation of PC into chitosan nanoparticle caused significant increment in intensity of –CH stretching peak 2960 (Hadidi et al., 2020), suggesting increase in ester content derived from PC components (Fig. 1 C). Moreover, most of the PC peaks were appeared in Nm-PC nanoparticles at same wave number illustrating successful encapsulation of PC as a core material inside the chitosan biopolymer.

Table 4
Encapsulation efficiency (EE), loading capacity (LC) and encapsulation yield (EY) of Nm-PC.

Chitosan/PC ratio (w/v)	Encapsulation efficiency (%)	Loading capacity (%)	Encapsulation yield (%)
1:0.0	0.00 ± 0.00^a	0.00 ± 0.00^a	
1:0.2	12.69 ± 0.69^b	0.15 ± 0.06^b	
1:0.4	29.26 ± 1.87^c	0.92 ± 0.11^c	
1:0.6	47.87 ± 2.54^d	1.79 ± 0.19^d	
1:0.8	82.99 ± 4.74^e	3.87 ± 0.87^e	25.78
1:1	71.58 ± 3.57^f	2.65 ± 0.49^f	

Note: Values are mean ($n = 3$) ± SE, the means followed by same letter in the same column are not significantly different according to ANOVA and Tukey's multiple comparison tests.

3.4.3. *Crystallinity study by X-ray diffractometry*

At the time of encapsulation, effect of PC on crystallographic structure of chitosan was determined by using XRD assay of chitosan powder, chitosan nanoparticle and Nm-PC nanoparticle (Fig. 1 D.). It is clearly evident that chitosan powder displayed crystalline region with strong reflection peak at 2θ value 20.10° which has been attributed due to intermolecular hydrogen bonding between NH_3^+ and –OH group of the chitosan chain itself suggesting the hydrated and regular crystal of chitosan (Liu and Liu, 2020). In case of unloaded chitosan nanoparticle

maximum declining of crystallinity was recorded that may be due to the cross-linking interaction of amino group of chitosan with phosphate group of S-TPP. However, PC caused effective decrement in chitosan crystallinity by reduction of peak intensity and widening of peak area after proper entrapment which may be corresponded to new intermolecular interaction between chitosan and PC functional groups reinforcing the destruction of chitosan crystallographic structures (Jahed et al., 2017). Increasing amorphous nature after significant interaction of PC with chitosan nanobiopolymer could suggest the application of Nm-PC nanoparticles as smart nano-delivery system for food preservation.

3.5. Determination of encapsulation efficiency (EE), loading capacity (LC) and encapsulation yield (EY)

EE simply represents the percentage of essential oil properly entrapped inside the chitosan nanocarrier, while, LC measures the weight of essential oil capable to be encapsulated into formed emulsionic particles depending on the amount of wall material used. EE and LC of Nm-PC for various chitosan to PC ratios (*w/v*) ranged between 12.69 and 82.99% and 0.15–3.87%, respectively (Table 4). There was a directly proportional relationship for increment in % EE and LC with increasing concentration of PC upto 1:0.8 ratio, followed by surprising decrement in EE and LC values. This suggests chitosan had limited potentiality to encapsulate PC as a core material. Moreover, higher concentration of PC might cause feeble adsorption at the surface of the chitosan nanocarrier leading to detachment of PC molecules during the collection of emulsionic particles by centrifugation (Amiri et al., 2021). The entrapment of essential oil into matrix polymer also depends on the affinity of component to be encapsulated and their diffusion in solvent during encapsulation process (Ghayempour et al., 2016). Some other factors like hydrophobic, hydrophilic, and resonance effect in essential oil components may also be responsible for charge attraction/repulsion leading to entrapment into matrix polymer (Janes et al., 2001). Similar finding with initial increment followed by decrement in % LC and EE has been reported by Hasheminejad et al. (2019) and Zhang et al. (2020), while encapsulating clove and tarragon essential oils into chitosan nanoparticles, respectively. Higher LC and EE values indicated the maximum entrapment of PC with better emulsion system stability.

EY of Nm-PC nanoemulsion was measured at maximum EE and LC values (1:0.8 ratio) and recorded to be 25.78%. Greater EY confirmed the successful encompassment of PC droplets inside chitosan nanomatrix with better compaction and stability. Our result is consistent with previous investigation of Das et al. (2021c) regarding encapsulation of linalool into chitosan nanocomposite with innovative delivery system, required for protection of stored food commodities against fungi, aflatoxin contamination and oxidative biodeterioration.

3.6. In vitro release of Nm-PC

In vitro release suggests the time dependent control volatilization of PC from chitosan nanoemulsion and amount of PC released was measured at 267 nm. In vitro PC release investigation was performed in PBS (pH 7.4) and ethanol mixture, because the system simulates with the stored food system. Basically, the release mechanism of essential oils depends on decomposition, surface erosion, desorption, diffusion and their subsequent delivery (Hasani et al., 2018). PC released from chitosan nanostructure has been categorized into two different steps viz. initial rapid followed by further sustained release up to a period of 0–192 h. In the present investigation, 38.02% release was recorded within first 8 h followed by 21.89 and 12.77% at 8–16 and 16–24 h, respectively (Fig. 2 A). After 96 h, very slow release (1.14%) was found with controlled delivery (Fig. 2 A), suggesting the usefulness of Nm-PC in preservation of food commodities having gradual fungitoxic and AFB_1 inhibitory activities. Initial burst release of PC was probably resulted due to adsorption of PC droplets on the surface of chitosan nanocarrier with rapid detachment during centrifugation. However, during later phase, the sustained leaching of PC from chitosan nanoemulsion might be attributed due to aqueous phase interaction of chitosan leading to emulsionic expansion followed by loosening the interaction little by little and controlled volatilization from the pore of the hydrocarbon surface (Hasani et al., 2018). Long term sustained delivery of essential oil has been associated with the slow diffusion of PC from PC loaded chitosan nanoemulsion. The penetration of buffer solution in emulsionic particles facilitated further polymer swelling and controlled release of PC synergistic formulation (Esmaeili and Asgari, 2015). In addition, it has also been reported that penetration of release medium into fabricated particles at pH 7.4 could modify the glossy polymeric structure of chitosan into rubbery state, thereby leading to long term diffusion of PC synergistic formulation into release medium (Soltanzadeh et al., 2021). Sustained delivery of entrapped PC synergistic formulation for longer time duration is more advantageous for shelf-life enhancement of stored food commodities. Amiri et al. (2020) also reported same pattern of biphasic release of cumin essential oil from chitosan nanoparticle with initial 22% release in first 5 h followed by slow release upto 160 h. However, our finding illustrated sustained release of PC components over a period of 192 h suggesting controlled delivery with long term maintenance of Nm-PC efficacy in stored food system, a prerequisite for gradual antifungal and antiaflatoxigenic effects.

3.7. Antifungal and AFB_1 inhibitory effectiveness of PC and Nm-PC

Inhibition of fungal growth and AFB_1 secretion was determined by MIC and MAIC assay and presented in Table 5. For in vitro determination of AFB_1 production, we have preferred thin layer chromatography (TLC) method because of increased amount of AFB_1 produced by *Aspergillus flavus* in liquid SMKY medium. Furthermore, it is also fast, less expensive, and widely used analytical method for mycotoxin quantification. The TLC method also requires comparatively lesser amount of organic solvents than high performance liquid chromatography (HPLC). PC inhibited the complete growth of AF LHP R14 cells and AFB_1 production at 0.2 and 0.15 μL/mL, respectively. Nm-PC showed better achievements in antifungal and AFB_1 inhibitory activities at 0.06 and 0.05 μL/mL, respectively. Moreover, effective inhibition of *A. candidus*, *A. luchuensis*, *A. sydowii*, *A. repens*, *Fusarium oxysporum*, *F. poae*, *Alternaria alternata*, and Mycelia sterilia cells growth were recorded at MIC doses of PC and Nm-PC, respectively (Fig. 2 B). Chitosan nanoemulsion did not exhibit prominent inhibitory effect against fungal growth (2.74%) and AFB_1 secretion (3.62%) (Table 5). Antifungal and AFB_1 inhibitory effectiveness of PC was found far better than individual PAEO and CSEO as well as other essential oils/bioactive components such as *Schinus molle* (López-Meneses et al., 2018) and eugenol (Das et al., 2021a), respectively. Better antifungal effectiveness of Nm-PC has been associated with synergistic activity of PC and chitosan in subcellular size emulsionic particles and disintegration of membrane function due to efficient interaction of phosphate, amine, terpene and hydroxyl groups of PC to negatively charge components of plasma membrane. Nm-PC mediated lower dose inhibition of AFB_1 biosynthesis as compared to fungal growth suppression might be corresponded with impairment in carbohydrate catabolism and inhibition of conidial germination. Moreover, controlled delivery of PC aroma from chitosan nanoemulsion may be a possible reason for effective diminution of norsolinic acid, a vital precursor of AFB_1 biosynthesis. Similar trend for improvement in antifungal and antiaflatoxigenic activities was reported by Singh et al. (2019) while encapsulating *Ocimum sanctum* essential oil into chitosan nanoparticle. The findings of our investigation promptly suggest tight packing of PC droplets inside chitosan nanomatrix facilitating targeted delivery at the phases and sub-phases of the stored food products where excessive fungal colonization were occurred in association with AFB_1 secretion (López-Meneses et al., 2018).

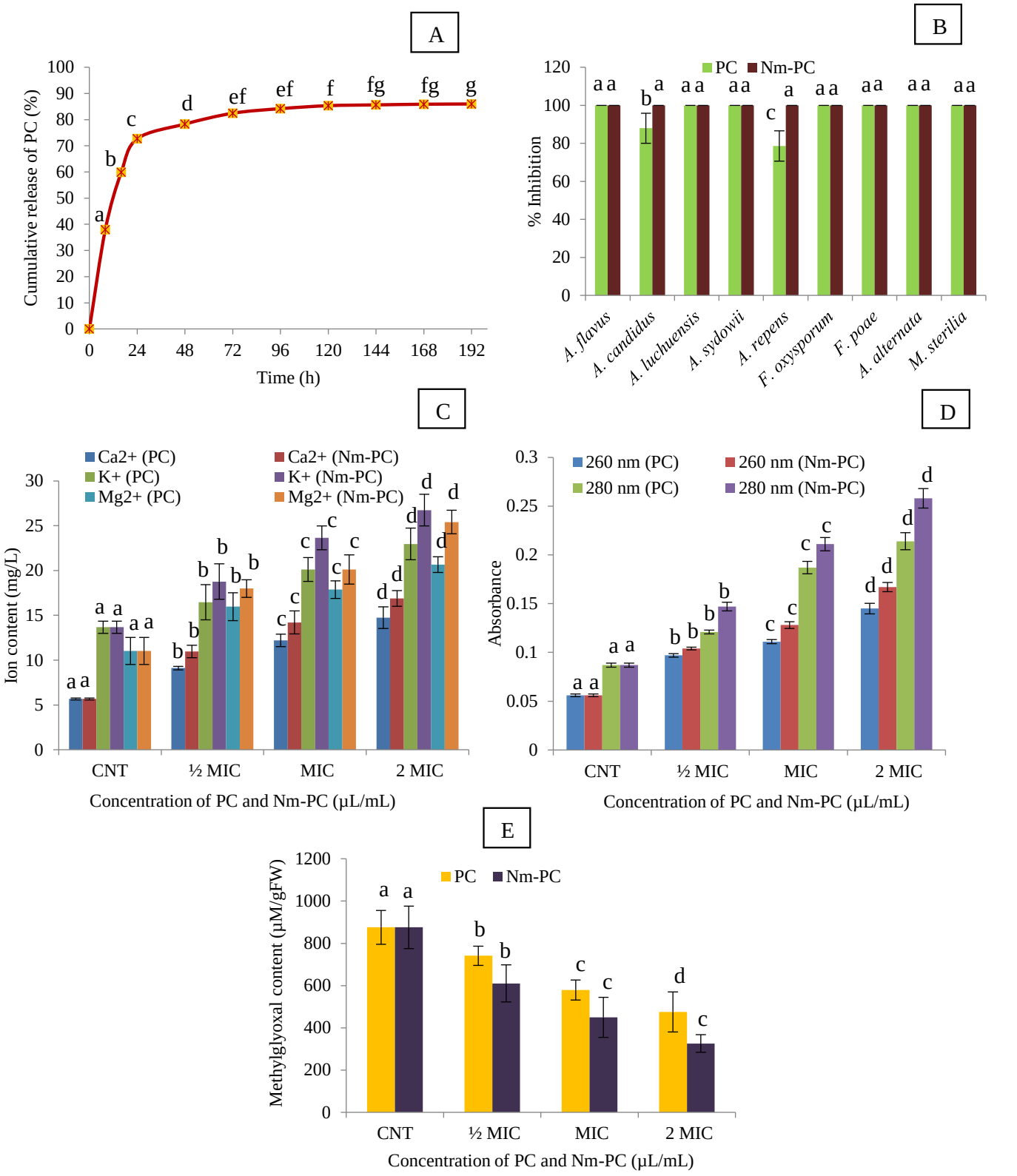

Fig. 2. In vitro release profile of Nm-PC (A), Fungitoxic spectrum of PC and Nm-PC against food contaminating fungi (B), Effect of PC and Nm-PC on leakage of Ca^{2+}, K^{+}, and Mg^{2+} ions from AF LHP R14 strain (C), Effect of PC and Nm-PC on leakage of 260 and 280 nm absorbing materials (D), Effect of PC and Nm-PC on cellular methylglyoxal (E).

Table 5
Effect of PC and Nm-PC on inhibition of fungal growth (AF LHP R14), AFB_1 and ergosterol production.

Concentration (μL/mL)	PC			Concentration (μL/mL)	Nm-PC		
	% inhibition of growth	% inhibition of AFB_1	% inhibition of ergosterol		% inhibition of growth	% inhibition of AFB_1	% inhibition of ergosterol
CNT	0.00 ± 0.00[a]	0.00 ± 0.00[a]	0.00 ± 0.00[a]	CNT	0.00 ± 0.00[a]	0.00 ± 0.00[a]	0.00 ± 0.00[a]
0.05	13.98 ± 1.87[b]	27.87 ± 2.97[b]	8.97 ± 1.71[b]	Chitosan nanoemulsion	2.74 ± 0.87[b]	3.62 ± 0.17[b]	1.98 ± 0.12[b]
0.1	54.20 ± 3.74[c]	61.68 ± 6.41[c]	47.20 ± 2.97[c]	0.01	11.96 ± 1.63[c]	17.96 ± 2.17[c]	17.69 ± 2.02[c]
0.15	86.84 ± 5.41[d]	100 ± 0.00[d]	78.63 ± 3.17[d]	0.02	38.97 ± 2.01[d]	46.32 ± 3.85[d]	41.65 ± 3.74[d]
0.2	100 ± 0.00[e]		100 ± 0.00[e]	0.03	57.98 ± 2.97[e]	63.78 ± 5.92[e]	79.02 ± 4.12[e]
				0.04	79.85 ± 4.87[f]	92.31 ± 3.65[f]	91.32 ± 2.98[f]
				0.05	87.20 ± 5.03[g]	100 ± 0.00[g]	100 ± 0.00[g]
				0.06	100 ± 0.00[h]		

Note: Values are mean (n = 3) ± SE, the means followed by same letter in the same column are not significantly different according to ANOVA and Tukey's multiple comparison tests.

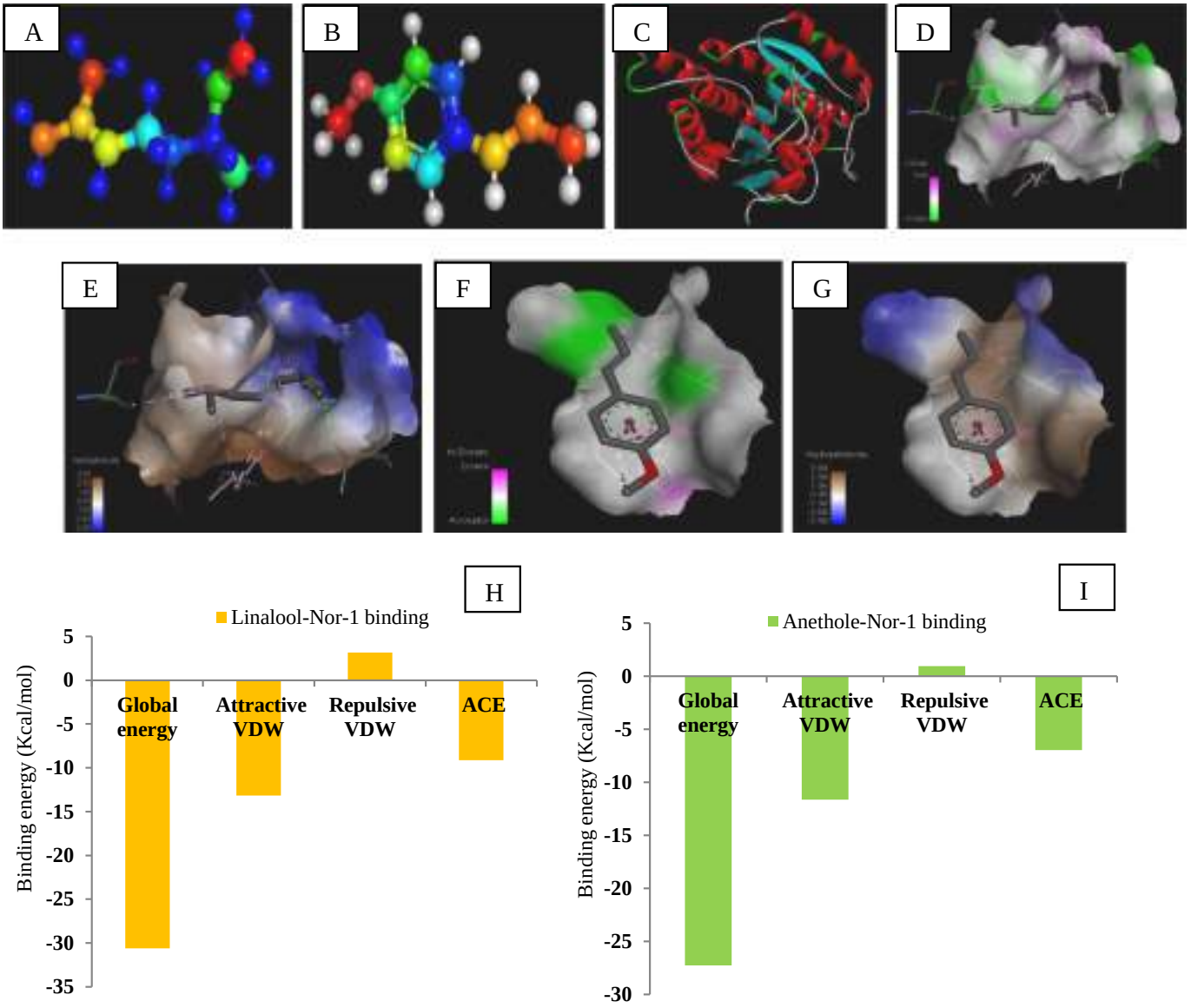

Fig. 3. 3D structure of linalool (A), anethole (B), Nor-1 protein (C), Hydrogen bond interaction of linalool with Nor-1 protein (D), Hydrophobic interaction of linalool with Nor-1 protein (E), Hydrogen bond interaction of anethole with Nor-1 protein (F), Hydrophobic interaction of anethole with Nor-1 protein (G), Binding energy indices of linalool-Nor-1 interaction (H), Binding energy indices of anethole-Nor-1 interaction (I).

3.8. Biochemical mechanisms involving antifungal and AFB_1 inhibition

PC and Nm-PC showed prominent in vitro antifungal and AFB_1 inhibitory efficacy, however, the actual mechanism specifying prime target site of action has been elucidated through biochemical and molecular mechanisms of action. Ergosterol is unique neutral lipid (sterol) molecule in fungal plasma membrane, participating in membrane fluidity, integrity and cellular viability (Li et al., 2021a). It is a useful target site for different antifungal drugs, based on this view; we have determined the total ergosterol content in AF LHP R14 cells after fumigation with PC and Nm-PC. In the present investigation, UV–visible spectrophotometry based ergosterol determination was carried out because the quantification method takes advantage of unique absorption spectra pattern of extracted sterol between 230 and 300 nm, which is indicative of the ergosterol and 24(28) dehydroergosterol [a late sterol pathway intermediate] content. Both, ergosterol and 24(28) dehydroergosterol absorb at 281.5 nm, whereas only 24(28) dehydroergosterol shows an intense spectral absorption band at 230 nm. Therefore, the amount of ergosterol can be determined by subtracting the absorbance value of 24(28) dehydroergosterol from total ergosterol. Moreover, UV–visible spectrophotometry based ergosterol determination is an easy and absolute measurement method without involvement of any expensive chemicals. PC displayed 8.97, 47.20, 78.63 and 100% inhibition of ergosterol at different concentrations of 0.05, 0.1, 0.15 and 0.2 μL/mL, respectively (Table 5). Nm-PC showed lower dose inhibition of ergosterol biosynthesis as compared to unencapsulated PC (Table 5). No marked inhibition of ergosterol biosynthesis was recorded by chitosan nanoemulsion (Table 5). Significant inhibition of ergosterol biosynthesis by PC fumigation may be due to dysfunction of several biosynthetic steps of ergosterol production especially by down-regulation of *ERG 11*, *ERG 6* and *ERG 4* genes leading to decrement in mRNA production as consistent with the previous investigation of Wei et al. (2020) regarding cinnamaldehyde mediated inhibition of ergosterol biosynthesis in *Fusarium sambucinum*. Moreover, the hydroxyl groups in essential oil components may have compensatory effect on ergosterol synthesis (Wan et al., 2019). Superior efficacy for inhibition of ergosterol production by Nm-PC might be associated with nanometric particle size with greater surface to volume ratio and aqueous phase solubility facilitating control delivery and better inhibition kinetics. Effective retardation in ergosterol content by *Origanum majorana* essential oil loaded chitosan nanoemulsion in *A. flavus* cells has been recently demonstrated by Chaudhari et al. (2020). However, the present result illustrated better achievement in ergosterol inhibition which supported the notion of exciting usefulness regarding application of Nm-PC for effective suppression of toxigenic fungal growth and AFB_1 mediated food biodeterioration.

Impairment in ergosterol molecule in plasma membrane by PC and Nm-PC fumigation could induce the leakage of vital ions, nucleic acids, and proteins leading to disruption of cellular homoeostasis. For confirming this hypothesis, effect of PC and Nm-PC on leakage of K^+, Mg^{2+} and Ca^{2+} ions and 260, 280 nm absorbing materials were observed. Exposure of PC and Nm-PC to AF LHP R14 cells led to maximum efflux of K^+, Mg^{2+} and Ca^{2+} ions (Fig. 2 C) and 260 (equivalent to nucleic acids), 280 nm (equivalent to proteins) absorbing materials (Fig. 2 D) at MIC and 2 MIC doses. Hydrophobic nature along with greater solubility after encapsulation of PC into chitosan nanoemulsion may be a possible reason for maximum entrance into *A. flavus* cells by crossing the membrane lipid bilayer (Li et al., 2021b) and severely affected the membrane porin proteins, which ultimately disturbed the major cellular organelles such as Endoplasmic reticulum, Golgi body and Endosomes required for AFB_1 biosynthesis and metabolism (Kistler and Broz, 2015).

For assessing the AFB_1 inhibitory mechanism of action, effect of PC and Nm-PC on cellular methyglyoxal was determined. Methylglyoxal is a dicarbonyl reactive byproduct of respiration having deleterious effects on foods by inducing aflatoxin contents which has been linked with up-regulation of *afl R*, *nor 1* and *ver 1* gene products and key substrates for synthesis of advance glycation end components after reaction with Arg, Lys and Gly amino acids of cellular proteins (Zheng et al., 2020; Das et al., 2021a). In the present piece of study, methylglyoxal level was inhibited at MIC (578.66 μM/gFW) and 2 MIC (475.33 μM/gFW) doses of PC as compared to control (875.96 μM/gFW) (Fig. 2 E). Nm-PC showed superior retardation in methylglyoxal synthesis at MIC and 2 MIC doses. PC mediated suppression of methylglyoxal production has been related to the benzene ring, –OH and –COOH group of phenolic and terpenoid components of PC molecules with effective trapping ability of cellular methylglyoxal, inhibition of reactive oxygen species production and electrophilic substitution causing the formation of PC-methylglyoxal adduct and reduced its occurrence (Lo et al., 2011; Yeh et al., 2017). Effective decrement of methylglyoxal by Nm-PC may be due to nanometric particles of emulsion system causing better reaction kinetics with controlled delivery at the target site. Hence, significant reduction in methylglyoxal has been correlated with novel antiaflatoxigenic mechanism of action and would be of exciting green image in food industries for development of aflatoxin resistant rice varieties by integrating sustainable green transgenic technology.

3.9. Molecular mechanism for AFB_1 inhibition: validation through in silico investigation

Molecular mechanism for inhibition of AFB_1 biosynthesis was elucidated by in silico homology docking study via targeting the Nor-1 protein and its interaction with anethole and linalool (found as major components of PC) (Fig. 3 A-I). Nor-1 protein was selected on the basis of its crucial role in conversion of norsolorinic acid to averantin in AFB_1 biosynthesis pathway. Three dimensional (3 D) structure of Nor-1 was modeled through Phyre 2 online server with 96% amino acid residues at >90% confidence (Model dimension (Å) = X: 54.461; Y: 53.398; Z: 43.497). The result of homology docking was analyzed on the basis of binding energy indices viz. global energy, attractive Van der Waal, repulsive Van der Waal's force and atomic contact energy (Fig. 3 H, I). Highest affinity of test components with receptor proteins related to more negative binding energies. Fig. 3 D, E, F, G represent that anethole and linalool efficiently interacted with different amino acids viz. Ala 113, Thr 218, and Arg 34 of Nor-1 proteins through hydrogen bond and hydrophobic interactions. Our result is consistent with the investigation of Das et al. (2021a) suggesting hydrogen bond dependent interaction of eugenol with Ver-1 protein of AFB_1 synthesis leading to specific alteration in stereo-spatial shapes of catalytic sides. Conclusively, effective binding of anethole and linalool with Nor-1 structural proteins revealed a green insight for laboratory synthesis of plant based bioactive components and support the hypothesis in terms of agricultural reference with betterment in inhibition of fungal infestation and AFB_1 mediated biodeterioration of stored food products.

3.10. Antioxidant activity

Fungal and AFB_1 contamination in stored foods may lead to oxidative deterioration by generation of reactive oxygen species (ROS) and lipid peroxidation. Hence, antioxidant activity of PAEO, CSEO, PC and Nm-

Table 6
Antioxidant activities of PAEO, CSEO, PC and Nm-PC.

Essential oil	DPPH (IC_{50}) μL/mL	ABTS (IC_{50}) μL/mL
PAEO	21.15 ± 2.02^a	17.51 ± 1.57^a
CSEO	17.87 ± 1.01^b	8.52 ± 0.41^b
PC	8.98 ± 0.69^c	2.65 ± 0.21^c
Nm-PC	5.29 ± 0.11^d	1.78 ± 0.08^d
Chitosan nanoemulsion	89.63 ± 3.58^e	78.21 ± 2.15^e

Note: Values are mean (n = 3) ± SE. The means followed by same letter in the same column are not significantly different according to ANOVA and Tukey's multiple comparison tests.
Absorbance of negative control for both assays was determined as 0% inhibition.

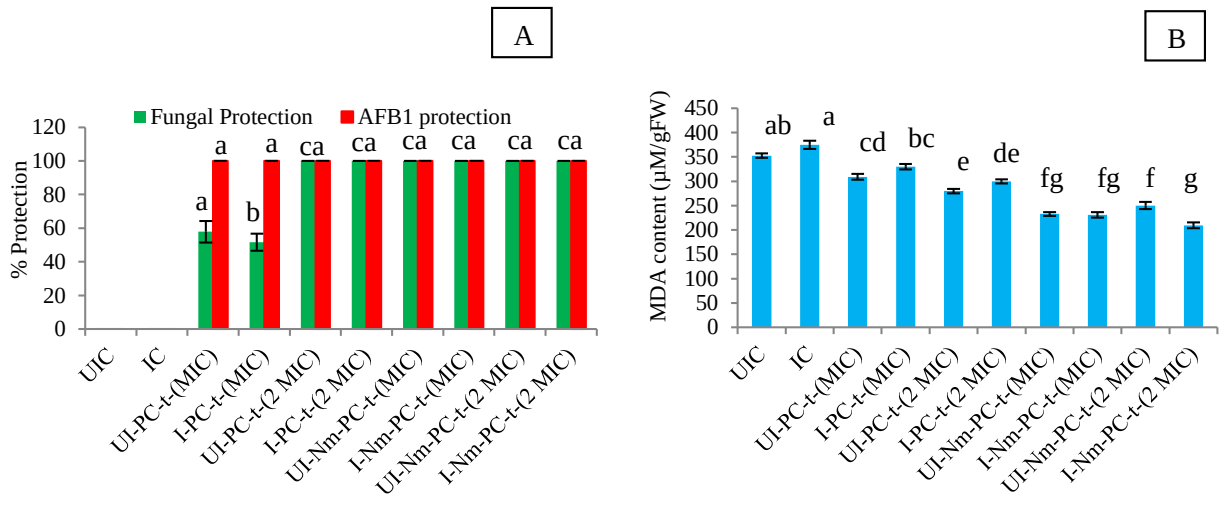

UIC = Uninoculated control

IC = Inoculated control

UI-PC-t-(MIC) = Uninoculated PC treatment (MIC)

I-PC-t-(MIC) = Inoculated PC treatment (MIC)

UI-PC-t-(2 MIC) = Uninoculated PC treatment (2 MIC)

I-PC-t-(2 MIC) = Inoculated PC treatment (2 MIC)

UI-Nm-PC-t-(MIC) = Uninoculated Nm-PC treatment (MIC)

I-Nm-PC-t-(MIC) = Inoculated Nm-PC treatment (MIC)

UI-Nm-PC-t-(2 MIC) = Uninoculated Nm-PC treatment (2 MIC)

I-Nm-PC-t-(2 MIC) = Inoculated Nm-PC treatment (2 MIC)

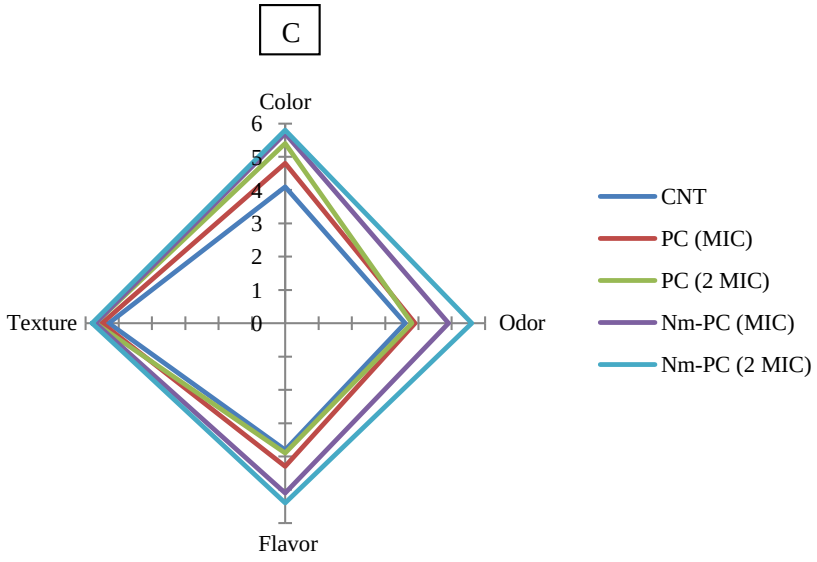

Fig. 4. In situ antifungal and AFB_1 inhibitory efficacy of PC and Nm-PC in rice (A), Effect of PC and Nm-PC on MDA content of rice (B), Effect of PC and Nm-PC on organoleptic properties of rice (C).

PC was measured through DPPH• and $ABTS^{\cdot+}$ free radical quenching assay. 50% scavenging effect (IC_{50}) of PC for DPPH• and $ABTS^{\cdot+}$ radicals was observed at 8.98 and 2.65 μL/mL, respectively. PC showed better free radical scavenging potentiality as compared to PAEO ($DPPH_{IC50}$ = 21.15 μL/mL, $ABTS_{IC50}$ = 17.51 μL/mL) and CSEO ($DPPH_{IC50}$ = 17.87 μL/mL, $ABTS_{IC50}$ = 8.52 μL/mL). Nanoencapsulation induced the antioxidant potentiality of PC with IC_{50} values 5.29 and 1.78 μL/mL for DPPH• and $ABTS^{\cdot+}$, respectively (Table 6). Chitosan nanoemulsion showed negligible antioxidant activity ($DPPH_{IC50}$ = 89.63 μL/mL, $ABTS_{IC50}$ = 78.21 μL/mL) which has been associated with involvement of amino groups in ionic gelation process of nanoemulsion synthesis (Das et al., 2021a). Superiority in antioxidant activity may be corresponded with synergistic interaction of chitosan and PC components leading to maximum free radical neutralization. Similar result with increased antioxidant activity of clove essential oil after entrapment in chitosan nanoparticle has been reported by Hadidi et al. (2020). Higher antioxidant activity may strengthen the application of Nm-PC as green antioxidant for stored food preservation in place of adverse effects of synthetic antioxidants.

3.11. *In situ efficacy of PC and Nm-PC against fungal infestation and AFB_1 contamination in rice (the model food system): high performance liquid chromatography (HPLC) analysis*

In situ efficacy of PC and Nm-PC was performed in rice (Kala joha variety) and inhibition of fungal infestation was measured through percent protection after one year of storage. Uninoculated and inoculated rice samples exhibited 57.88 and 51.71% protection against fungal infestation at the MIC dose of PC, respectively (Fig. 4 A). Complete protection against fungal proliferation was observed at 2 MIC dose of PC. However, Nm-PC completely inhibited fungal association at both MIC and 2 MIC doses. In our present investigation, for detection of AFB_1 in stored rice seeds, HPLC method was used because AFB_1 was present in quite small quantity that can't be quantified precisely by TLC. AFB_1 content in uninoculated and inoculated control rice samples were recorded as 23.69 and 21.58 μg/kg, respectively, which exceeded the maximum limit prescribed by European Regulatory Commission (Commission Regulation (EU) No.165/2010, 2010). Both, PC and Nm-PC showed 100% inhibition of AFB_1 biosynthesis after one year of storage (Fig. 4 A). The in vitro MIC dose of PC was not able to provide complete fungal protection because some of the volatile components might be absorbed by rice itself lowering its bioefficacy in real food system (Tian et al., 2012). Better antifungal and AFB_1 inhibitory efficacy of Nm-PC in stored rice has been associated with nano-size of emulsionic particles with greater solubility, controlled delivery and facilitated diffusion at different phases and sub-phases of rice seeds with intended inhibition of fungal conidial germination and AFB_1 biosynthesis. Interestingly, chitosan has the prominent potentiality to increase the stability of essential oils which has been attributed due to surface charge and increasing viscosity in dispersed phase of nanoemulsion (Chuah et al., 2009). More importantly, the in vitro inhibition of methylglyoxal (AFB_1 inducer) may support the notion of superior efficacy for AFB_1 inhibition in rice, presenting a green horizon with exciting significance for practical application of Nm-PC nanoemulsion as novel green food preservative. A recent investigation suggested the efficacy of cinnamon essential oil nanoemulsion with effective inhibition of *Fusarium graminearum* infestation (100% protection) and 3-acetyldeoxynivalenol (0.2 μg/g) and deoxynivalenol (0.1 μg/g) production in rice culture over a period of 7 days of storage (Wu et al., 2019). However, our results demonstrated complete protection of rice seeds against fungi and AFB_1 mediated biodeterioration upto a period of one year, strengthening the application of Nm-PC nanoemulsion as smart nano-based control delivery vehicle in food and agricultural industries.

3.12. *Effect of PC and Nm-PC on lipid peroxidation of rice seeds*

Excessive fungal infestation and AFB_1 production in the storage conditions may lead to peroxidation of polyunsaturated fatty acids (PUFA) of rice into different volatile compounds such as hexanal, 2-pentylfuran, and 2-nonenal and secondary lipid hydroaldehydes viz. malondialdehyde (MDA) facilitating major oxidative burden along with nutritional deterioration (Das et al., 2021a; Choi et al., 2019). More importantly, rheology, charge, permeability, oxygen sensitivity, pH and fatty acid composition of food determine the extent of lipid peroxidation during storage periods (Waraho et al., 2011). In the present piece of study, lipid peroxidation in control and fumigated (PC and Nm-PC) rice seeds were measured in terms of MDA production due to efficient interaction with TBA forming colored MDA-TBA adduct. Much higher MDA level was recognized for uninoculated (345.26 μM/gFW) and inoculated (374.69 μM/gFW) rice samples. PC fumigation at MIC and 2 MIC doses significantly inhibited MDA biosynthesis (Fig. 4 B) which has been associated with effective free radical neutralization capacity, restraining the terminal oxidation of fatty acids (Bajpai et al., 2015). Nm-PC displayed superiority over its unencapsulated form for retardation of MDA biosynthesis at MIC and 2 MIC doses in rice (Fig. 4 B). Better efficacy of Nm-PC for inhibition of MDA biosynthesis may be due to nanometric emulsionic particles providing greater surface area, which had maximum scavenging potentiality of free radicals and superior reaction kinetics for inhibition of terminal fatty acid oxidation. Shokri et al. (2020) demonstrated effective retardation of lipid peroxidation in rainbow trout fillets by *Ferulago angulata* essential oil loaded chitosan nanoemulsion upto 16 days of storage periods. However, our result illustrated superiority for inhibition of lipid peroxidation in rice by keeping low level of MDA over a period of one year, facilitating the application of Nm-PC nanoemulsion as effective green food preservative.

3.13. *Effect of PC and Nm-PC on organoleptic properties of rice seeds*

Oxidative stress along with lipid peroxidation during storage conditions may cause possible interference in color, odor, flavor and texture of rice. Therefore, evaluation of organoleptic properties through hedonic scale in control and fumigated (PC and Nm-PC) rice seeds represented the consumer acceptance with wide scale practical utility. It is possible to observe from Fig. 4 C, maximum changes in flavor and odor in control sets by reducing the acceptable limit that may be due to oxidative deterioration of food nutritional components producing volatile lipid peroxides. PC fumigated rice seeds at 2 MIC doses displayed intense aroma that might be associated with absorption of volatile components and ultimate declining in hedonic scores. Fumigation of rice seeds with Nm-PC at MIC and 2 MIC doses showed satisfactory scores for color, odor, flavor and texture of rice as compared to control groups. Investigation of Deepika et al. (2021) evaluated the fumigation of *Petroselinum crispum* essential oil and its nanoformulation to chia seeds and observed the greater sensory acceptance at lower concentration i.e. MIC dose, a result in accordance with our present findings. Conclusively, it can be demonstrated that the Nm-PC promoted fungal inhibition in rice during storage without significantly affecting the organoleptic attributes, illustrating its practical applicability as green food preservative against fungal and AFB_1 contamination.

3.14. *Assessment of LD_{50} in mice (animal model)*

Safety assessment of PC and Nm-PC was presented in terms of LD_{50} (50% lethality) in mice and values were recorded as 13,659 and 10,587 μL/kg body weight, respectively. The LD_{50} values were recognized much higher than prevalently used commercial preservatives such as benzoic acid (2000–2500 mg/kg), formic acid (700 mg/kg), fonophos and parathion (1–25 mg/kg) (Isman, 2006). Somewhat decrement in LD_{50} for Nm-PC during acute oral toxicity in mice may be due to nanometric

size of emulsionic particles with greater surface absorption and toxicity. More importantly, higher LD_{50} as compared to OECD prescribed limit (5000 mg/kg) confirmed the practical application of Nm-PC as safe eco-smart nano-green food preservative.

4. Conclusion

Encompassment of PC synergistic formulation into chitosan nano-biopolymer improved the antifungal, antiaflatoxigenic and antioxidant activities as compared to unencapsulated PC. Controlled volatilization of PC from chitosan nanomatrix facilitated long term protection of rice against fungal infestation, AFB_1 production, and ROS mediated biodeterioration. The investigation also explored the biochemical mechanisms for inhibition of fungal growth and diminution of methylglyoxal production, a prerequisite for mitigation of AFB_1 contamination, directing the future integration of Nm-PC synergistic formulation in developing aflatoxin resistant rice varieties by green transgenic technology. In silico modeling advocated the molecular interaction of linalool and anethole with Nor-1 protein leading to inhibition of AFB_1 biosynthesis. Moreover, strong in situ antifungal, antiaflatoxigenic efficacy, lipid peroxidation suppressing potentiality, acceptable organoleptic properties in rice and mammalian non-toxicity recommend the application of nanoencapsulated PC synergistic mixture formulation as natural, eco-smart nano-green food preservative.

Declaration of Competing Interest

Authors reported no conflict of interest.

Acknowledgements

Somenath Das is thankful to Council of Scientific and Industrial Research (CSIR) [File No.: 09/013(0774)/2018-EMR-I], New Delhi, India, for the financial support. The authors wish to thank the head and coordinator CAS in Botany, DST-FIST, DST-PURSE, ISLS, and CIFC-IIT, Banaras Hindu University (BHU) and Principal, Burdwan Raj College, Purba Bardhaman, West Bengal, India for laboratory facilities.

References

Al-Zoreky, N.S., Saleh, F.A., 2019. Limited survey on aflatoxin contamination in rice. Saudi J. Biol. Sci. 26 (2), 225–231. https://doi.org/10.1016/j.sjbs.2017.05.010.

Amiri, A., Mousakhani-Ganjeh, A., Amiri, Z., Guo, Y.G., Singh, A.P., Kenari, R.E., 2020. Fabrication of cumin loaded-chitosan particles: characterized by molecular, morphological, thermal, antioxidant and anticancer properties as well as its utilization in food system. Food Chem. 310, 125821 https://doi.org/10.1016/j.foodchem.2019.125821.

Amiri, A., Ramezanian, A., Mortazavi, S.M.H., Hosseini, S.M.H., Yahia, E., 2021. Shelf-life extension of pomegranate arils using chitosan nanoparticles loaded with Satureja hortensis essential oil. J. Sci. Food Agric. 101 (9), 3778–3786. https://doi.org/10.1002/jsfa.11010.

Bahmankar, M., Mortazavian, S.M.M., Tohidfar, M., Noori, S.A.S., Darbandi, A.I., Alfekaiki, D.F., 2019. Chemotypes and morpho-physiological characters affecting essential oil yield in Iranian cumin landraces. Ind. Crop. Prod. 128, 256–269. https://doi.org/10.1016/j.indcrop.2018.10.080.

Bajpai, V.K., Sharma, A., Kim, S.H., Baek, K.H., 2015. Chemical composition, antioxidant, lipid peroxidation inhibition and free radical scavenging activities of microwave extracted essential oil from *Allium sativum*. J. Essent. Oil-Bear. Plants. 18 (2), 300–313. https://doi.org/10.1080/0972060X.2013.764215.

Barrera-Martínez, C.L., Padilla-Vaca, F., Liakos, I., Melendez-Ortiz, H.I., Cortez-Mazatan, G.Y., Peralta-Rodríguez, R.D., 2021. Chitosan microparticles as entrapment system for trans-cinnamaldehyde: synthesis, drug loading, and *in vitro* cytotoxicity evaluation. Int. J. Biol. Macromol. 166, 322–332. https://doi.org/10.1016/j.ijbiomac.2020.10.188.

Buege, J.A., Aust, S.D., 1978. [30] Microsomal lipid peroxidation. In: Methods in Enzymology, vol. 52. Academic press, pp. 302–310. https://doi.org/10.1016/S0076-6879(78)52032-6.

Burdock, G.A., Carabin, I.G., 2009. Safety assessment of coriander (*Coriandrum sativum* L.) essential oil as a food ingredient. Food Chem. Toxicol. 47 (1), 22–34. https://doi.org/10.1016/j.fct.2008.11.006.

Chaudhari, A.K., Singh, V.K., Das, S., Prasad, J., Dwivedy, A.K., Dubey, N.K., 2020. Improvement of in vitro and in situ antifungal, AFB1 inhibitory and antioxidant activity of *Origanum majorana* L. essential oil through nanoemulsion and recommending as novel food preservative. Food Chem. Toxicol. 143, 111536 https://doi.org/10.1016/j.fct.2020.111536.

Chaudhari, A.K., Singh, V.K., Das, S., Dubey, N.K., 2022. Fabrication, characterization, and bioactivity assessment of chitosan nanoemulsion containing allspice essential oil to mitigate *Aspergillus flavus* contamination and aflatoxin B_1 production in maize. Food Chem. 372, 131221 https://doi.org/10.1016/j.foodchem.2021.131221.

Choi, S., Seo, H.S., Lee, K.R., Lee, S., Lee, J., Lee, J., 2019. Effect of milling and long-term storage on volatiles of black rice (*Oryza sativa* L.) determined by headspace solid-phase microextraction with gas chromatography–mass spectrometry. Food Chem. 276, 572–582. https://doi.org/10.1016/j.foodchem.2018.10.052.

Chuah, A.M., Kuroiwa, T., Kobayashi, I., Nakajima, M., 2009. Effect of chitosan on the stability and properties of modified lecithin stabilized oil-in-water monodisperse emulsion prepared by microchannel emulsification. Food Hydrocoll. 23 (3), 600–610. https://doi.org/10.1016/j.foodhyd.2008.03.014.

Clemente, I., Aznar, M., Nerín, C., 2019. Synergistic properties of mustard and cinnamon essential oils for the inactivation of foodborne moulds *in vitro* and on Spanish bread. Int. J. Food Microbiol. 298, 44–50. https://doi.org/10.1016/j.ijfoodmicro.2019.03.012.

da Silva Gündel, S., de Souza, M.E., Quatrin, P.M., Klein, B., Wagner, R., Gündel, A., Ourique, A.F., 2018. Nanoemulsions containing Cymbopogon flexuosus essential oil: development, characterization, stability study and evaluation of antimicrobial and antibiofilm activities. Microb. Pathog. 118, 268–276. https://doi.org/10.1016/j.micpath.2018.03.043.

Das, S., Singh, V.K., Dwivedy, A.K., Chaudhari, A.K., Upadhyay, N., Singh, A., Dubey, N. K., 2019. Antimicrobial activity, antiaflatoxigenic potential and *in situ* efficacy of novel formulation comprising of *Apium graveolens* essential oil and its major component. Pestic. Biochem. Physiol. 160, 102–111.

Das, S., Singh, V.K., Dwivedy, A.K., Chaudhari, A.K., Upadhyay, N., Singh, A., Dubey, N. K., 2020. Assessment of chemically characterized *Myristica fragrans* essential oil against fungi contaminating stored scented rice and its mode of action as novel aflatoxin inhibitor. Nat. Prod. Res. 34 (11), 1611–1615. https://doi.org/10.1080/14786419.2018.1519826.

Das, S., Singh, V.K., Dwivedy, A.K., Chaudhari, A.K., Dubey, N.K., 2021a. Eugenol loaded chitosan nanoemulsion for food protection and inhibition of Aflatoxin B_1 synthesizing genes based on molecular docking. Carbohydr. Polym. 255, 117339 https://doi.org/10.1016/j.carbpol.2020.117339.

Das, S., Singh, V.K., Dwivedy, A.K., Chaudhari, A.K., Dubey, N.K., 2021b. Insecticidal and fungicidal efficacy of essential oils and nanoencapsulation approaches for the development of next generation ecofriendly green preservatives for management of stored food commodities: an overview. Int. J. Pest Manag. 1-32 https://doi.org/10.1080/09670874.2021.1969473.

Das, S., Singh, V.K., Chaudhari, A.K., Dwivedy, A.K., Dubey, N.K., 2021c. Fabrication, physico-chemical characterization, and bioactivity evaluation of chitosan-linalool composite nano-matrix as innovative controlled release delivery system for food preservation. Int. J. Biol. Macromol. 181, 751–763. https://doi.org/10.1016/j.ijbiomac.2021.08.045.

Deepika, Chaudhari, A.K., Singh, A., Das, S., Dubey, N.K., 2021. Nanoencapsulated *Petroselinum crispum* essential oil: characterization and practical efficacy against fungal and aflatoxin contamination of stored chia seeds. Food Biosci. 42, 101117 https://doi.org/10.1016/j.fbio.2021.101117.

Devi, S.M., Raj, N., Sashidhar, R.B., 2021. Efficacy of short-synthetic antifungal peptides on pathogenic Aspergillus flavus. Pestic. Biochem. Physiol. 174, 104810 https://doi.org/10.1016/j.pestbp.2021.104810.

Esmaeili, A., Asgari, A., 2015. In vitro release and biological activities of Carum copticum essential oil (CEO) loaded chitosan nanoparticles. Int. J. Biol. Macromol. 81, 283–290. https://doi.org/10.1016/j.ijbiomac.2015.08.010.

Gavahian, M., Sastry, S., Farhoosh, R., Farahnaky, A., 2020. Ohmic heating as a promising technique for extraction of herbal essential oils: Understanding mechanisms, recent findings, and associated challenges. In: Advances in Food and Nutrition Research, vol. 91. Academic Press, pp. 227–273.

Ghayempour, S., Montazer, M., Rad, M.M., 2016. Encapsulation of Aloe Vera extract into natural Tragacanth Gum as a novel green wound healing product. Int. J. Biol. Macromol. 93, 344–349. https://doi.org/10.1016/j.ijbiomac.2016.08.076.

Hadidi, M., Pouramin, S., Adinepour, F., Haghani, S., Jafari, S.M., 2020. Chitosan nanoparticles loaded with clove essential oil: characterization, antioxidant and antibacterial activities. Carbohydr. Polym. 236, 116075 https://doi.org/10.1016/j.carbpol.2020.116075.

Hasani, S., Ojagh, S.M., Ghorbani, M., 2018. Nanoencapsulation of lemon essential oil in chitosan-Hicap system. Part 1: study on its physical and structural characteristics. Int. J. Biol. Macromol. 115, 143–151. https://doi.org/10.1016/j.ijbiomac.2018.04.038.

Hashem, A.S., Awadalla, S.S., Zayed, G.M., Maggi, F., Benelli, G., 2018. *Pimpinella anisum* essential oil nanoemulsions against Tribolium castaneum—insecticidal activity and mode of action. Environ. Sci. Pollut. Res. 25 (19), 18802–18812. https://doi.org/10.1007/s11356-018-2068-1.

Hasheminejad, N., Khodaiyan, F., Safari, M., 2019. Improving the antifungal activity of clove essential oil encapsulated by chitosan nanoparticles. Food Chem. 275, 113–122. https://doi.org/10.1016/j.foodchem.2018.09.085.

Hosseini, S.F., Zandi, M., Rezaei, M., Farahmandghavi, F., 2013. Two-step method for encapsulation of oregano essential oil in chitosan nanoparticles: preparation, characterization and in vitro release study. Carbohydr. Polym. 95 (1), 50–56. https://doi.org/10.1016/j.carbpol.2013.02.031.

Houicher, A., Hamdi, M., Hechachna, H., Özogul, F., 2018. Chemical composition and antifungal activity of Anacyclus valentines essential oil from Algeria. Food Biosci. 25, 28–31. doi:https://doi.org/10.1016/j.fbio.2018.07.005.

Isman, M.B., 2006. Botanical insecticides, deterrents, and repellents in modern agriculture and an increasingly regulated world. Annu. Rev. Entomol. 51, 45–66. https://doi.org/10.1146/annurev.ento.51.110104.151146.

Jahed, E., Khaledabad, M.A., Almasi, H., Hasanzadeh, R., 2017. Physicochemical properties of *Carum copticum* essential oil loaded chitosan films containing organic nanoreinforcements. Carbohydr. Polym. 164, 325–338. https://doi.org/10.1016/j.carbpol.2017.02.022.

Janes, K.A., Fresneau, M.P., Marazuela, A., Fabra, A., Alonso, M.J., 2001. Chitosan nanoparticles as delivery systems for doxorubicin. J. Control. Release. 73 (2–3), 255–267. https://doi.org/10.1016/S0168-3659(01)00294-2.

Kaur, N., Chahal, K.K., Kumar, A., Singh, R., Bhardwaj, U., 2019. Antioxidant activity of Anethum graveolens L. essential oil constituents and their chemical analogues. J. Food Biochem. 43 (4), e12782 https://doi.org/10.1111/jfbc.12782.

Kistler, H.C., Broz, K., 2015. Cellular compartmentalization of secondary metabolism. Front. Microbiol. 6, 68–84. https://doi.org/10.3389/fmicb.2015.00068.

Kumar, A., Singh, P.P., Prakash, B., 2020. Unravelling the antifungal and anti-aflatoxin B_1 mechanism of chitosan nanocomposite incorporated with *Foeniculum vulgare* essential oil. Carbohydr. Polym. 236, 116050 https://doi.org/10.1016/j.carbpol.2020.116050.

Lesjak, M., Simin, N., Orcic, D., Franciskovic, M., Knezevic, P., Beara, I., Mimica-Dukic, N., 2016. Binary and tertiary mixtures of *Satureja hortensis* and *Origanum vulgare* essential oils as potent antimicrobial agents against *Helicobacter pylori*. Phytother. Res. 30 (3), 476–484. https://doi.org/10.1002/ptr.5552.

Li, Y., Dai, M., Zhang, Y., Lu, L., 2021a. The sterol C-14 reductase Erg24 is responsible for ergosterol biosynthesis and ion homeostasis in *Aspergillus fumigatus*. Appl. Microbiol. Biotechnol. 105 (3), 1253–1268. https://doi.org/10.1007/s00253-021-11104-5.

Li, J., Fu, S., Fan, G., Li, D., Yang, S., Peng, L., Pan, S., 2021b. Active compound identification by screening 33 essential oil monomers against *Botryosphaeria dothidea* from postharvest kiwifruit and its potential action mode. Pestic. Biochem. Physiol. 104957 https://doi.org/10.1016/j.pestbp.2021.104957.

Liu, T., Liu, L., 2020. Fabrication and characterization of chitosan nanoemulsions loading thymol or thyme essential oil for the preservation of refrigerated pork. Int. J. Biol. Macromol. 162, 1509–1515. https://doi.org/10.1016/j.ijbiomac.2020.07.207.

Lo, C.Y., Hsiao, W.T., Chen, X.Y., 2011. Efficiency of trapping methylglyoxal by phenols and phenolic acids. J. Food Sci. 76 (3), H90–H96. https://doi.org/10.1111/j.1750-3841.2011.02067.

López-Meneses, A.K., Plascencia-Jatomea, M., Lizardi-Mendoza, J., Fernández-Quiroz, D., Rodríguez-Félix, F., Mouriño-Pérez, R.R., Cortez-Rocha, M.O., 2018. *Schinus molle* L. essential oil-loaded chitosan nanoparticles: preparation, characterization, antifungal and anti-aflatoxigenic properties. LWT 96, 597–603. https://doi.org/10.1016/j.lwt.2018.06.013.

Matshetshe, K.I., Parani, S., Manki, S.M., Oluwafemi, O.S., 2018. Preparation, characterization and in vitro release study of β-cyclodextrin/chitosan nanoparticles loaded *Cinnamomum zeylanicum* essential oil. Int. J. Biol. Macromol. 118, 676–682. https://doi.org/10.1016/j.ijbiomac.2018.06.125.

Nikkhah, M., Hashemi, M., 2020. Boosting antifungal effect of essential oils using combination approach as an efficient strategy to control postharvest spoilage and preserving the jujube fruit quality. Postharvest Biol. Technol. 164, 111159 https://doi.org/10.1016/j.postharvbio.2020.111159.

Nikkhah, M., Hashemi, M., Najafi, M.B.H., Farhoosh, R., 2017. Synergistic effects of some essential oils against fungal spoilage on pear fruit. Int. J. Food Microbiol. 257, 285–294. https://doi.org/10.1016/j.ijfoodmicro.2017.06.021.

Piaru, S.P., Mahmud, R., Majid, A.M.S.A., Nassar, Z.D.M., 2012. Antioxidant and antiangiogenic activities of the essential oils of *Myristica fragrans* and *Morinda citrifolia*. Asian Pac J Trop Med 5 (4), 294–298. https://doi.org/10.1016/S1995-7645(12)60042-X.

Reyes-Jurado, F., Cervantes-Rincón, T., Bach, H., López-Malo, A., Palou, E., 2019. Antimicrobial activity of Mexican oregano (*Lippia berlandieri*), thyme (*Thymus vulgaris*), and mustard (*Brassica nigra*) essential oils in gaseous phase. Ind. Crop. Prod. 131, 90–95. https://doi.org/10.1016/j.indcrop.2019.01.036.

Shanakhat, H., Sorrentino, A., Raiola, A., Romano, A., Masi, P., Cavella, S., 2018. Current methods for mycotoxins analysis and innovative strategies for their reduction in cereals: an overview. J. Sci. Food Agric. 98 (11), 4003–4013. https://doi.org/10.1002/jsfa.8933.

Sheijooni-Fumani, N., Hassan, J., Yousefi, S.R., 2011. Determination of aflatoxin B1 in cereals by homogeneous liquid–liquid extraction coupled to high performance liquid chromatography-fluorescence detection. J. Sep. Sci. 34 (11), 1333–1337. https://doi.org/10.1002/jssc.201000882.

Shokri, S., Parastouei, K., Taghdir, M., Abbaszadeh, S., 2020. Application an edible active coating based on chitosan-Ferulago angulata essential oil nanoemulsion to shelf life extension of Rainbow trout fillets stored at 4 C. Int. J. Biol. Macromol. 153, 846–854. https://doi.org/10.1016/j.ijbiomac.2020.03.080.

Singh, V.K., Das, S., Dwivedy, A.K., Rathore, R., Dubey, N.K., 2019. Assessment of chemically characterized nanoencapuslated Ocimum sanctum essential oil against aflatoxigenic fungi contaminating herbal raw materials and its novel mode of action as methyglyoxal inhibitor. Postharvest Biol. Technol. 153, 87–95. https://doi.org/10.1016/j.postharvbio.2019.03.022.

Soltanzadeh, M., Peighambardoust, S.H., Ghanbarzadeh, B., Mohammadi, M., Lorenzo, J. M., 2021. Chitosan nanoparticles encapsulating lemongrass (*Cymbopogon commutatus*) essential oil: physicochemical, structural, antimicrobial and in-vitro release properties. Int. J. Biol. Macromol. 192, 1084–1097. https://doi.org/10.1016/j.ijbiomac.2021.10.070.

Songsamoe, S., Matan, N., Matan, N., 2017. Antifungal activity of Michelia alba oil in the vapor phase and the synergistic effect of major essential oil components against *Aspergillus flavus* on brown rice. Food Control 77, 150–157. https://doi.org/10.1016/j.foodcont.2017.02.010.

Tian, J., Huang, B., Luo, X., Zeng, H., Ban, X., He, J., Wang, Y., 2012. The control of Aspergillus flavus with *Cinnamomum jensenianum* Hand.-Mazz essential oil and its potential use as a food preservative. Food Chem. 130 (3), 520–527. https://doi.org/10.1016/j.foodchem.2011.07.061.

Upadhyay, N., Singh, V.K., Dwivedy, A.K., Das, S., Chaudhari, A.K., Dubey, N.K., 2018. Cistus ladanifer L. essential oil as a plant based preservative against molds infesting oil seeds, aflatoxin B_1 secretion, oxidative deterioration and methylglyoxal biosynthesis. Lwt 92, 395–403. https://doi.org/10.1016/j.lwt.2018.02.040.

Walia, S., Mukhia, S., Bhatt, V., Kumar, R., Kumar, R., 2020. Variability in chemical composition and antimicrobial activity of Tagetes minuta L. essential oil collected from different locations of Himalaya. Ind. Crop. Prod. 150, 112449 https://doi.org/10.1016/j.indcrop.2020.112449.

Wan, J., Zhong, S., Schwarz, P., Chen, B., Rao, J., 2019. Physical properties, antifungal and mycotoxin inhibitory activities of five essential oil nanoemulsions: impact of oil compositions and processing parameters. Food Chem. 291, 199–206. https://doi.org/10.1016/j.foodchem.2019.04.032.

Waraho, T., McClements, D.J., Decker, E.A., 2011. Mechanisms of lipid oxidation in food dispersions. Trends Food Sci. Technol. 22 (1), 3–13. https://doi.org/10.1016/j.tifs.2010.11.003.

Wei, J., Bi, Y., Xue, H., Wang, Y., Zong, Y., Prusky, D., 2020. Antifungal activity of cinnamaldehyde against *Fusarium sambucinum* involves inhibition of ergosterol biosynthesis. J. Appl. Microbiol. 129 (2), 256–265. https://doi.org/10.1111/jam.14601.

Wu, D., Lu, J., Zhong, S., Schwarz, P., Chen, B., Rao, J., 2019. Effect of chitosan coatings on physical stability, antifungal and mycotoxin inhibitory activities of lecithin stabilized cinnamon oil-in-water emulsions. LWT. 106, 98–104. https://doi.org/10.1016/j.lwt.2019.02.029.

Yadav, S.K., Singla-Pareek, S.L., Ray, M., Reddy, M.K., Sopory, S.K., 2005. Methylglyoxal levels in plants under salinity stress are dependent on glyoxalase I and glutathione. Biochem. Biophys. Res. Commun. 337 (1), 61–67. https://doi.org/10.1016/j.bbrc.2005.08.263.

Yeh, W.J., Hsia, S.M., Lee, W.H., Wu, C.H., 2017. Polyphenols with antiglycation activity and mechanisms of action: a review of recent findings. J. Food Drug Anal. 25 (1), 84–92. https://doi.org/10.1016/j.jfda.2016.10.017.

Zhang, H., Liang, Y., Li, X., Kang, H., 2020. Effect of chitosan-gelatin coating containing nano-encapsulated tarragon essential oil on the preservation of pork slices. Meat Sci. 166, 108137 https://doi.org/10.1016/j.meatsci.2020.108137.

Zheng, J., Guo, H., Ou, J., Liu, P., Huang, C., Wang, M., Xiao, J., 2020. Benefits, deleterious effects and mitigation of methylglyoxal in foods: a critical review. Trends Food Sci. Technol. 107, 201–212. https://doi.org/10.1016/j.tifs.2020.10.031.